AN INVISCID MODEL FOR PREDICTING UNSTEADY FORCES IN DOUBLY CONNECTED DOMAINS

Manimendra Acharige Chanaka Krishan Gunarathna

(138054 J)

Degree of Master of Science

Department of Mechanical Engineering

University of Moratuwa

Sri Lanka

March 2016

DECLARATION OF THE CANDIDATE & SUPERVISOR

I declare that this is my own work and this thesis does not incorporate without acknowledgement any material previously submitted for a Degree or Diploma in any other University or institute of higher learning and to the best of my knowledge and belief it does not contain any material previously published or written by another person expect where the acknowledgment is made in text.

Also, I hereby grant to University of Moratuwa the non-exclusive right to reproduce and distribute my thesis, in whole or in part in print, electronic or other medium. I retain the right to use this content in whole or part in future works (Such as articles or books)

……………………………..   Date: ………………………….

 M.A.C.K. Gunarathna

The above candidate has carried out research for the Masters thesis under my supervision.

……………………………..   Date: ………………………….

 Dr. W.K. Wimalsiri

……………………………..   Date: ………………………….

 Dr. V.P.C. Dassanayake

i

Abstract

Inviscid analytical-numerical model for predicting unsteady forces on two aerofoil configurations is developed and validated with the past literature. First the unsteady inviscid, incompressible and irrotational, except the logarithmic singularities at vortex points, flow field around the doubly connected domain is evaluated using a conformal mapping method. A discrete vortex shedding mechanism is incorporated to model the free shear layers of the real fluid flow. The complex potential associated with uniform flow and the vortex motion is obtained using elliptic functions and the modified Green's function respectively. The strengths of the vortices are evaluated using Kutta condition which keeps the regularity of the flow field. Circulation development around the aerofoils is quantified by utilizing Kelvin's circulation theorem. The unsteady forces are obtained using the unsteady version of the Blasius equation. Both trapezoidal rule and finite difference method are incorporated to solve the unsteady Blasius equation. The developed inviscid model is applied to various aerofoil configurations to predict the unsteady forces on the aerofoils. The results obtained were validated to the past relevant literature. Results showed a good agreement with the past literature.

Keywords: unsteady, forces, plunging, analytical-numerical, doubly

The work is dedicated to my parents

ACKNOWLEDGEMENT

TABLE OF CONTENTS

LIST OF FIGURES

1. <u>INTRODUCTION</u>

1.1. <u>Background</u>

Aerodynamics of wing configurations in aircrafts has been a field of increasing interest since the first powered flight with a canard biplane wing configuration, designed by Wright brothers in 1903. A vast improvement of the aircraft designs over the last century can be observed due to the improvements of the aerodynamic analyses of different types of aerofoil adaptations for the wing configurations. Scientists have paid their attention to the investigations of multi element wing systems, especially different types of biplane wing configurations, to improve the aerodynamic performance of the manned/ unmanned flights rather than only relying on the monoplane wing configurations. Investigations of the aerodynamic performance of the aerofoils in tandem biplane configuration date back since Prandtl work on biplane theory [1]. Indeed, many studies have demonstrated high aerodynamic performances of the biplane wing configuration over monoplane configuration [2]. Tandem biplane configurations provide many aerodynamic advantages for the aircrafts especially when it comes to military applications where there's a requirement of long range and endurance due to the low induced drag [3]. Also some of the analyses on dual wing systems for high performance business airplanes concluded that those systems provide more fuel efficiency compared with the monoplane systems since they experience lower induced drag than monoplanes due to a combination of two and three dimensional drag reduction and the structural advantage of the biplane wing configuration over the mono plane wing configuration. These studies also showed that tandem and unstaggered aerofoil configurations obtain high lift to drag ratios of these than that of monoplane configurations [4].

Recent advancements of the micro air vehicles (MAVs), which have wing span of less than 15cm [5] and can be used in a variety of military and civilian situations [6, 7], lead to analyze the flight of the insects. Flapping motion of the insect flight can be categorized such as pitching motion, plunging motion and combined pitch and plunge

motion. The objective in the current research community is to find out a better aerofoil adaptation and a better flapping motion mechanism for the MAVs. The wing configurations such as unstaggered biplane and tandem aerofoils are very important when considering a proper aerofoil adaptation for the MAVs and understanding the superior flight performance of the insect flight. There are basically two dimensionless parameters that have to be considered when analyzing insect flight, namely, reduced frequency and Strouhal number. The unsteadiness of the flapping flight is quantified by a dimensionless number called the reduced frequency (k) while the efficiency is quantified by the Strouhal number (St).

$$k = \frac{\omega c}{U_\infty} \tag{1}$$

$$St = \frac{2fh_0}{U_\infty} \tag{2}$$

where ω, f, c, h_0 and U_∞ are angular frequency, flapping frequency, chord length of the aerofoil, flapping amplitude and the free stream velocity respectively [5]. Smaller birds flies at higher reduced frequencies while larger birds flies at lower reduced frequencies meaning that the smaller birds tend fly at more unsteady conditions. Furthermore, based on the data of different species of insects, bats and birds in cruise flight, Taylor et al. [8] concluded that the Strouhal numbers of their flight lie within 0.2-0.4 while the average value being 0.29.

Many experimental and numerical methods were used to analyze the aerodynamic performance of the biplane wing configurations. However, there's a scarcity of theoretical models developed to analyze these kinds of biplane problems [9]. Major disadvantages of the direct numerical simulation (DNS) methods when analyzing these problems are the computational time. Therefore these problems should be analyzed using analytical models which are known to be computationally economical.

Compared to DNS methods, the vortex panel method and conformal mapping method reduce the computational cost while capturing accurate description of the fluid flow. The problem with the vortex panel method is that when the vortex particles are too close to the boundary, unrealistic results are obtained [10]. Also substantial and non-physical edge effects are present at the end of the each panel [11]. These kinds of deficiencies do not arise in conformal mapping technique since the no flow boundary condition is applied on the whole boundary. The method of images is valid even if the vortices are very close to the body. Also the conformal mapping technique is computationally economical than the vortex panel method. Therefore it is logical to analyze the problem using the conformal mapping technique.

1.2. <u>Overview</u>

The main objective of the study is to analyze aerodynamic performance of tandem, stationary/moving biplane wing configurations using a model which is computationally economical. Since the evaluation of lift and drag on the aerofoils are vital in these kinds of problems, the unsteady forces on the each aerofoil in the biplane configurations are evaluated by using two dimensional inviscid, incompressible, irrotational potential flow theory where the flow field consists of logarithmic point singularities at vortex points. First the aerofoils are mapped into a circular domain using a multiply connected domain conformal mapping method proposed by [12]. Then the complex potential associated with the uniform flow is determined using elliptic functions in doubly connected domain by mapping the mapped circular domain to a rectangular domain. Since a vortex shedding mechanism is incorporated to model the free shear layers of the fluid flow, the complex potential associated with vortex motion is evaluated by the modified Green's function [13] in the doubly connected domain. These complex potentials are combined to obtain total complex potential of the system. Then using unsteady Blasius equation, [14], [15] the complex forces are evaluated. Eventually the results obtained by the developed model are validated by the relevant literature and several doubly connected problems are analyzed using the developed model. This analysis can be considered as an extension of the study [16] even though the method used for the evaluation free stream complex potential is different in the current study compared with [16].

2. <u>LITERATURE REVIEW</u>

2.1. <u>Tandem aerofoil configuration</u>

A tandem aerofoil configuration is comprised of two independent lift generating aerofoils such that the aerofoils are on two different planes, separated vertically and horizontally. This type of aerofoil configuration has been a main aspect of the manned flight since the beginning. A tandem aerofoil configuration is shown in figure 1 with some valuable parameters.
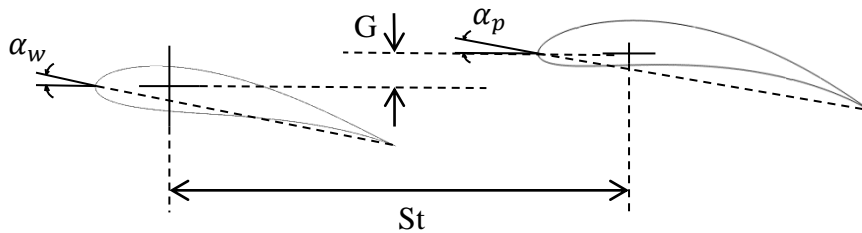
Figure 1: Tandem aerofoils: Stagger, Gap and Decalage

Specifically there are two types of tandem tail-wing configurations named canard wing configuration and delanne wing configuration. In a canard wing configuration, there is a small forewing ahead of the main wing in a tandem configuration. When there is a tail wing rear to the main wing, that type of tandem configuration is called delanne wing configuration.

Stagger, Gap and Decalage are defined as follows [17];

Stagger (St):

Stagger is defined as the distance between the forewing and rear wing 0.25 chord positions non dimensionalised by the chord. Stagger is positive when forewing is above the rear wing. Stagger is negative in figure 1.

Gap (G):

The absolute value of the vertical distance between the forewing 0.25 chord location and the rear wing 0.25 chord location non dirnensionalised by the chord is defined as the gap between aerofoils. By definition, the gap is always positive.

Decalage (δ):

Relative angle of attack between forewing and rear wing is defined as the decalage.

$$\delta = \alpha_w - \alpha_p \tag{3}$$

where α_w is the angle of attack of the forewing and α_p is the angle of the rearwing by the free stream.

There are many applications of tandem aerofoil configuration mainly in military aircrafts and home built aircrafts. To achieve high efficiency, long range and high flying, tandem aerofoil configurations are used in UAVs and modern fighter jets.

2.2. Pitching motion

An aerofoil that has a sinusoidal angular motion about its axis is considered to be in pitching motion. The angular displacement (α) and the angular velocity ($\dot{\alpha}$) of the pitching aerofoil is mathematically represented by Eq. (4) and Eq. (5). An aerofoil undergoing a pitching motion is shown in figure 2.

$$\alpha = \alpha_0 \cos(\omega t) \tag{4}$$

$$\dot{\alpha} = -\alpha_0 \omega \sin(\omega t) \tag{5}$$

Here α_0, ω and t are pitching amplitude, angular frequency of the pitching motion and time respectively.
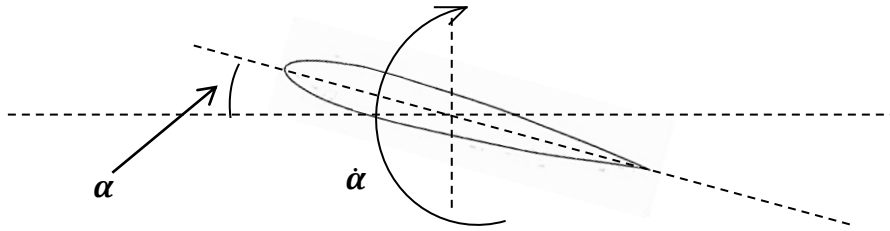
Figure 2: Pitching aerofoil

2.3. **Plunging aerofoil**

An aerofoil that has a sinusoidal translation motion about a fixed reference axis is considered to be in plunging motion. The displacement (h) and the translation velocity ($\dot{h}$) of the plunging aerofoil is mathematically represented by Eq. (6) and Eq. (7). An aerofoil undergoing a pitching motion is shown in figure 3.

$$h = h_0 cos(\omega t) \tag{6}$$

$$\dot{h} = -h_0 \omega sin(\omega t) \tag{7}$$
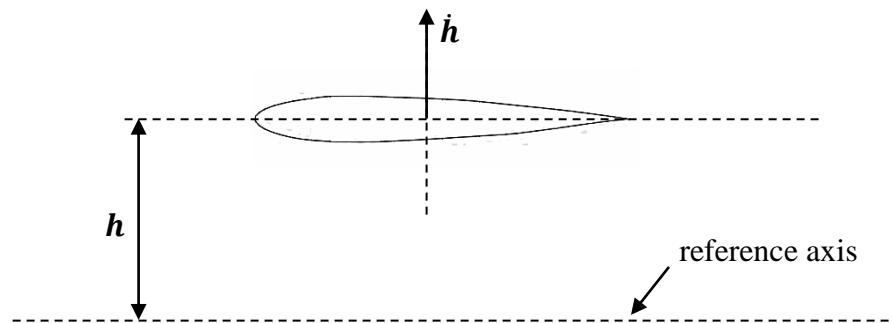
Figure 3: Plunging aerofoil

2.4. **Flapping aerofoils**

Many studies are available on the aerodynamic analysis of aerofoils undergoing flapping motion. These studies mainly concerned about the lift and thrust generation of the

flapping aerofoil and flapping aerofoil combinations since the mechanisms of lift and thrust generation are of main importance in this area of study.

The bird's ability to generate thrust by wing flapping was first observed by Knoller [18] and Betz [19] independently. As shown in the figure 4, an effective angle of attack is created, when an aerofoil flaps, resulting in a force having a lift force and a thrust force as its components. This phenomenon is called the Knoller-Betz effect. Katzmayr [20] was the first to analyze Knoller-Betz effect by experimentally analyzing the thrust on an aerofoil in a sinusoidally oscillating flow field.
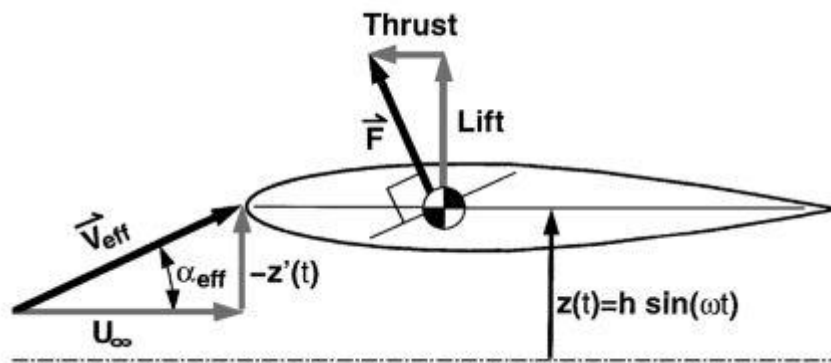
Figure 4: Thrust generation of a plunging aerofoil [21]

Von Karman and Burgers [22] theoretically analyzed the wake structures of plunging aerofoils and observed that the location and the polarity of the wake vortices indicate whether the wake structure is drag producing or thrust producing. Drag producing and thrust producing wake structures are shown in the figure 5 and figure 6 respectively. The theoretical analysis on the pitching and plunging aerofoils done by Garrick [23] concluded that an aerofoil undergoing a plunging motion produces thrust for any frequency range while an aerofoil undergoing a pitching motion produces thrust above a certain frequency and the trust generation depends on the location of the pitch axis of the aerofoil. Jones et al. [21] investigated the Knoller-Betz effect using experimental and computational methods. In their study, the vorticity structures and the time averaged velocity profiles of the wake were analyzed using inviscid unsteady panel codes. Yao et

8

al. [24] developed an inviscid unsteady model based on panel method for analyzing vortex-aerofoil-wake interaction problems. Aerofoils at tandem were analyzed using the model by obtaining flow patterns and unsteady forces for different kinds of configurations.
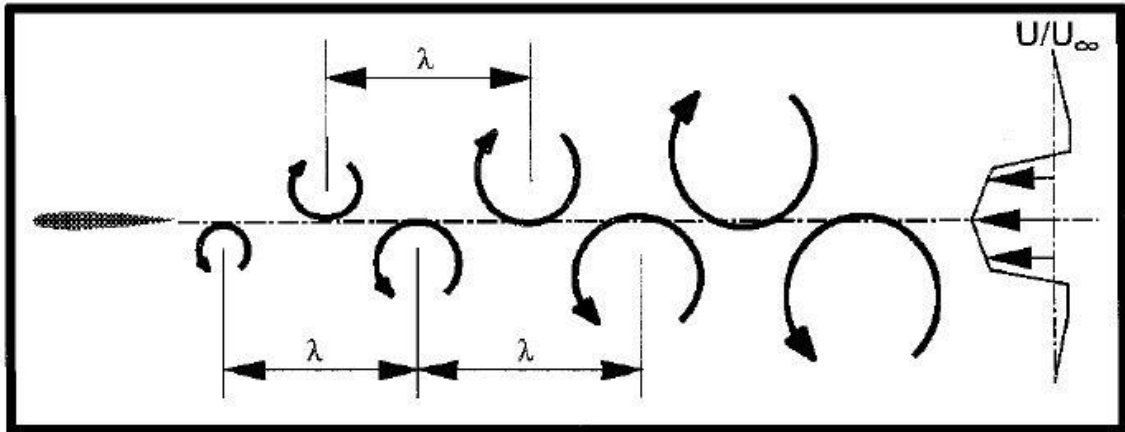
Figure 5: Drag producing wake pattern [21]
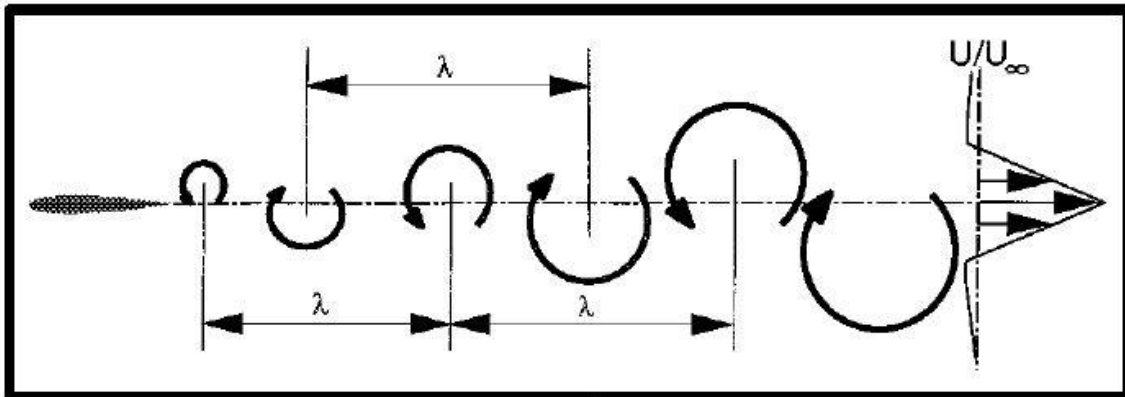
Figure 6: Thrust producing wake pattern [21]

Aziz and Mukherjee [25] obtained unsteady forces and wake structures of the two aerofoils in tandem. A potential flow model was used to model the flow field and to obtain unsteady forces. The results were validated with the literature.

2.5. <u>Analytical solutions for doubly connected problems</u>

2.5.1. <u>Uniform flow in doubly connected domain</u>

The analytical solution for the complex potential associated with the uniform flow (free stream) is well known when it comes to flow fields around a single contour in the unbounded fluid domain (simply connected domain). However, when there is more than a single contour in the fluid region, construction of the complex potential, analytically, becomes very complicated. There are several early investigations on the analytical solutions for the inviscid, irrotational and incompressible flow fields in doubly connected domains (two contours in the fluid domain).

Hicks [26] obtained the analytical solution for the flow field when two cylinders are in arbitrary motion. Velocity potential was obtained by definite integrals and when the motion of the cylinders are restricted such that they move as a whole like a rigid body, the solution for the flow field was obtained using elliptic functions and bipolar coordinates. The same problem was addressed by Greenhill [27] and the flow solution was obtained as an infinite series in bipolar coordinates. Carpenter [28] obtained an analytical flow solution, as an infinite series in rectangular coordinates, for two cylinders in real axis. Using the same method, Kawaguti [29] solved the problem of two cylinders moving past each other.

Flow fields around two obstacles, with specifiable circulations around those, were investigated by Lagally [30] and Ferrari [31], independently, using elliptic functions. The solution for the flow field was represented by Weierstrass zeta functions and Weierstrass sigma functions [32]. Solution for the uniform flow field was obtained in terms of Weierstrass zeta functions. Using Lagally's approach, Garrick [33] analyzed the flow field around a biplane configuration with the use of proper conformal mapping. Wang [34] obtained the flow solutions for the unsteady flow field around two arbitrarily translating and expanding circles by using conformal mapping and Fourier series.

Crowdy [35] introduced a generalized method, mainly by utilizing a special transcendental function called Schottky Klein prime function [36], [37], to obtain the flow field around any finite number of cylindrical objects in uniform flow when the circulations around the obstacles are taken to be vanished. The method introduced can be extended to any general shaped bodies if the conformal mapping from the bounded canonical multiply connected region to the unbounded fluid region is known.

2.5.2. <u>Vortex motion in doubly connected domain</u>

Early investigations on vortex dynamics are mainly by Kirchhoff and Routh [38]. Lin [39], [40] was the first to extend the Kirchhoff Routh approach to vortex motion in multiply connected domains.

Johnson and Mcdonald [41] addressed the problem of vortex motion in doubly connected domain. A problem that has significance in geophysical fluid dynamics, motion of a vortex near two circles with arbitrary radii, was analyzed using Hamiltonion dynamics. The circulations around the circles were assumed to be null in the study. Further they analytically investigated a doubly connected problem of vortices near barrier gaps.

Zannetti et al. [42] addressed the problem of vortex motion in doubly connected domain when multiple vortices are present using elliptic functions. Vortex shedding of two element aerofoil and a two bladed Darrieus turbine were considered. They analyzed the patterns of flow fields and variation of the circulations around the aerofoils with time.

Crowdy and Marshall [43] developed a new constructive method for analyzing the movement of a point vortex near any finite number of obstacles in the fluid domain while taking circulations around the obstacles to be vanished. They have used the Hamiltonion dynamics to analyze the problem and also Kirchhoff Routh path functions [44] were reproduced in terms of Schottky Klein prime function due to its efficacy. Further, Crowdy [13] developed a new calculus for two dimensional vortex dynamics in multiply connected domains. By utilizing the new calculus, instantaneous complex

potentials can be evaluated when there are a finite number of vortices around finite number of arbitrary shaped obstacles. Furthermore, the freedom of specifying arbitrary values of circulations around the obstacles is also facilitated.

3. <u>MODEL DEVELOPMENT</u>

3.1. <u>Conformal mapping in doubly connected domains</u>

The problem involves with two NACA 0012 aerofoils in tandem configuration. Since the aerofoil shapes are complicated, those shapes must be conformally mapped into a circular computational domain which is an annulus region. This is achieved by series of mapping functions. First, the aerofoils are mapped, conformally, into two disjoint circles using a holomorphic function, $z = z(v)$, by utilizing a method for conformal mapping of multiply connected domains proposed by M.E. Klonowska and W.J. Prosnak [12] as in the study [16]. Then the disjoint circles are mapped into an annulus region.

3.1.1. <u>Conformal mapping from physical plane to circular domain</u>

The conformal map is from physical z **-** plane to v **-** plane. Existence of a mapping function, $z = z(v)$, is ensured by Koebe theorem [45] which states that every multiply connected domain can be mapped into a circular domain with the same connectivity. The uniqueness of the solution is obtained by following normalizing conditions as mentioned in the same theorem.

- It is assumed that the mapping is one to one. Therefore, when $z \to \infty, v \to \infty$ and $z(\infty) = \infty$.

- It is also assumed that the directions in the two points at infinity of the mapping planes are identical. Hence,

$$\frac{dz}{dv}\bigg|_{z=\infty} = 1.$$

3.1.1.1. <u>Standard form of the mapping function</u>

According to Runge theorem, any holomorphic function, $z(v)$, can be represented in a multiply connected domain by a sequence of rational functions that converges to $z(v)$. Therefore,

$$z = v + \sum_{k=1}^{K} \sum_{n=1}^{N_k} I_{kn} \left(\frac{a_k}{v - v_k} \right)^n \tag{8}$$

where,

$k \in [1, K]$

$K = 2$ (Number of bodies)

$N_k = 50$ (Truncated value)

I_{kn} - Complex constants associated with the mapping function

a_k - Radii of the mapped circles in v plane

v_k – Centers of the circles in v plane

Here the unknown constants, a_k, v_k, and I_{kn} are determined by the method proposed by [12]. Note that N_k, truncated value is taken to be 50 since the function z, converges at that value.

The equation (8) represents the mapping function from the two aerofoils in z – plane (physical domain), as shown in figure 7, into two disjoint circles in v – plane as shown in figure 8. Also, parameters when $k = 1,2$ represent the parameters of the circles that was mapped by the front aerofoil and the rear aerofoil respectively.
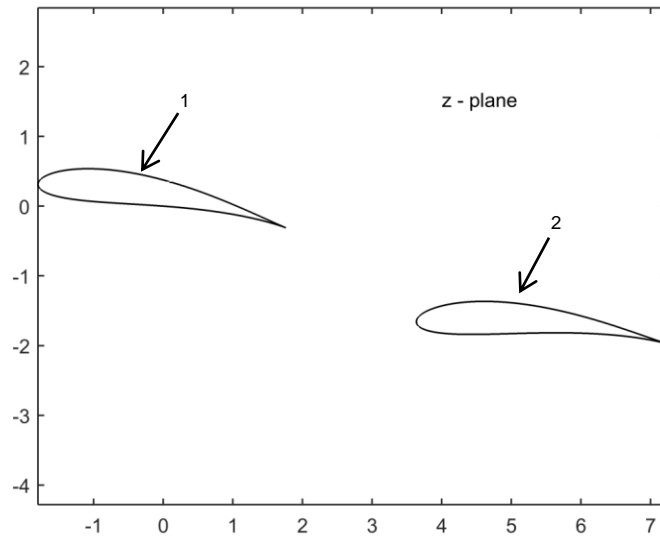
Figure 7: Aerofoils in z – plane (physical domain)
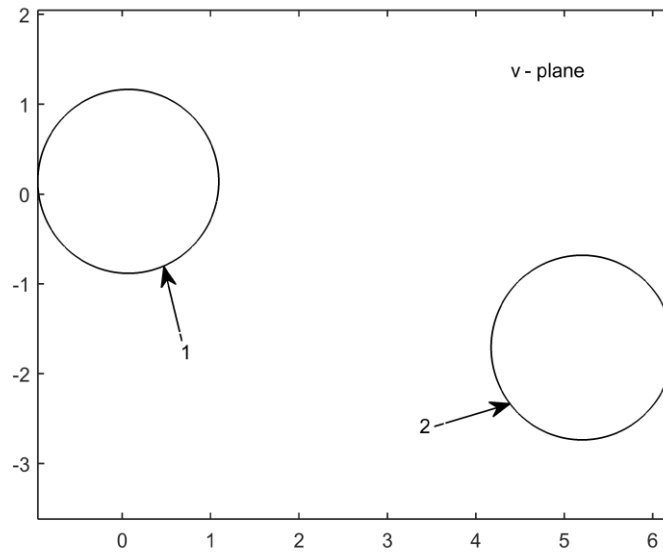
Figure 8: Mapped disjoint circles in v – plane, circle numbered as '1' corresponds to the front aerofoil and the other circle corresponds to rear aerofoil.

3.1.2. <u>Mapping functions</u>

Since the computational domains are an annulus and a rectangular domain, these domains are obtained using series of mapping functions.

The lower circle of the v-plane is mapped into V_1 - plane, using the equation (9), so that the center of the circle is at the origin of V_1 - plane. Also the upper circle is mapped accordingly.

$$V_1 = \left(\frac{v - v_2}{a_2} \right) \tag{9}$$

Next, by the transformation (10), the center of the circle corresponding to the upper aerofoil is taken to the real axis. Here α is the angle between the real axis and the line connecting the origin and the center of the circle corresponding to the upper aerofoil.

$$V_2 = V_1 . e^{-i\alpha} \tag{10}$$

Then V_2 - plane is transformed to the w - plane to make the circles, Apollonius circles, by the transformation (11).

$$w = \frac{V_2 - d}{c} \tag{11}$$

where,

$$d = \left(\left(|v_1 - v_2|^2 - \left(\frac{a_1}{a_2} \right)^2 + 1 \right) \middle/ 2|v_1 - v_2| \right)$$

$$c = \sqrt{(|v_1 - v_2| - d)^2 - a_1{}^2}$$

Then, w - plane is mapped to the ζ' - plane by the mapping function (12).

$$\zeta' = \left(\frac{w + 1}{w - 1} \right) \tag{12}$$

16

Finally, ζ' - plane (figure 9) is mapped into computational domains, ζ and τ, separately since the complex potential associated with uniform flow is evaluated in τ domain and the complex potential associated with vortex motion is evaluated in ζ domain.

ζ' - plane to ζ - plane (figure 10) and τ – plane (figure 11) transformations are obtained by the mapping functions (13) and (14) respectively.

$$\zeta = k\zeta' \tag{13}$$
$$\tau = \log(\zeta') \tag{14}$$

where k is a constant that makes outer circle unit radius and also $\zeta \to k$ maps $z \to \infty$. From ζ'- plane to ζ - plane, only the radii of the outer and inner circles are changed.
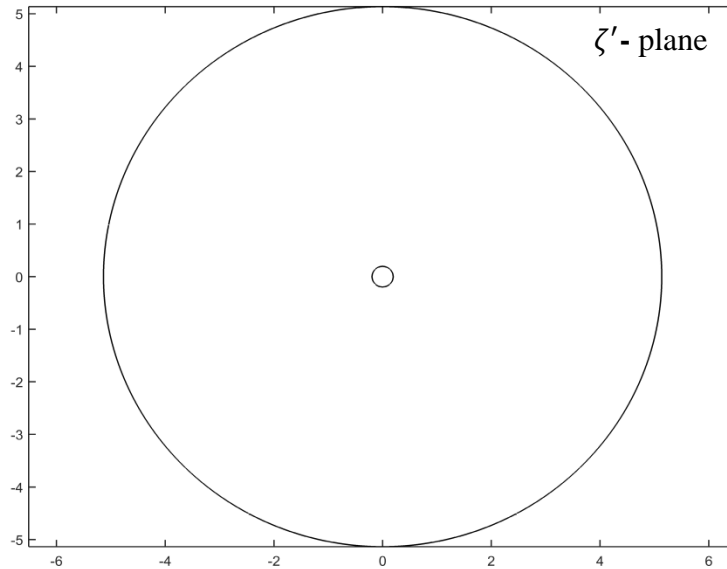
*Figure 9: ζ'- plane (Annulus region): front aerofoil is mapped into the outer circle while rear aerofoil is mapped into the inner circle in tandem configuration.
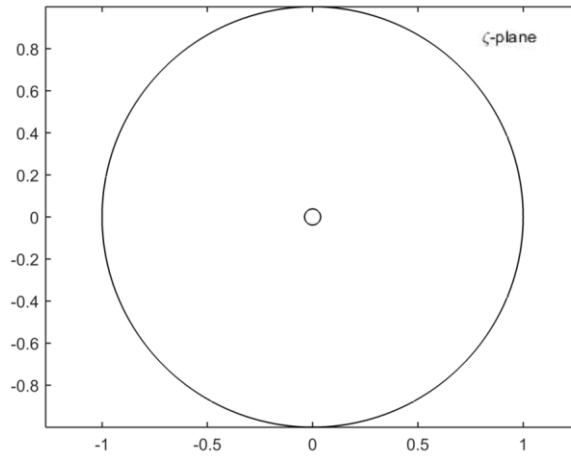
Figure 10: computational ζ - plane: front aerofoil is mapped into the outer circle while rear aerofoil is mapped into the inner circle.
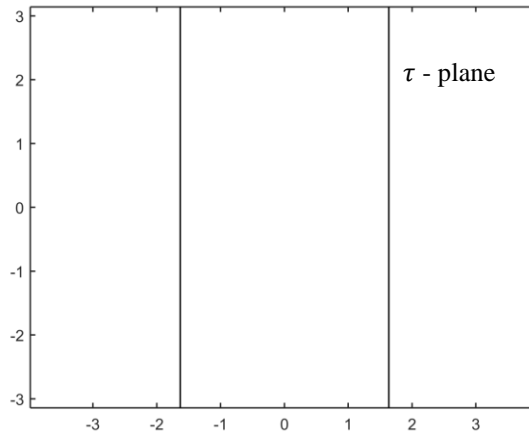
Figure 11: computational τ - plane: front aerofoil is mapped into the line in the right and the rear aerofoil is mapped into the line in the left in tandem configuration.

3.2. Evaluation of complex potential

3.2.1. Potential flow theory

The tandem biplane problem is addressed by two dimensional potential flow theory with the association of conformal mapping. The following assumptions are made.

- Inviscid fluid

- Incompressible fluid

- Irrotational fluid

Also the fluid domain contains point singularities due to the vortex motion that is used to model the free shear layers of the real fluid flow.

3.2.1.1. Governing equations

3.2.1.1.1. Incompressibility condition

By the continuity equation,

$$\frac{\partial \rho}{\partial t} + \nabla(\rho \vec{U}) = 0 \tag{15}$$

Where,

ρ - density of the fluid

$\vec{U}$ - velocity vector field

Since the flow field is assumed to be incompressible, the density of the fluid is constant. Therefore, ρ is constant. Hence the equation (15) can be written as equation (16);

$$\nabla \vec{U} = 0 \tag{16}$$

(i.e. divergence of the velocity vector field vanishes)

$\vec{U}$ can be represented as, $\vec{U} = u\boldsymbol{i} + v\boldsymbol{j}$, where $\boldsymbol{i}$ and $\boldsymbol{j}$ are unit vectors along x and y axes respectively and u, v are corresponding velocity components.

Then by the equation (16),

$$\frac{\partial u}{\partial x} + \frac{\partial v}{\partial y} = 0 \tag{17}$$

3.2.1.1.2. <u>Irrotationality condition</u>

Vorticity ($\boldsymbol{\eta}$) of a fluid flow field is defined as the local spin of a fluid particle.

$$\boldsymbol{\eta} = \nabla \times \vec{U} = 2\boldsymbol{\omega} \tag{18}$$

Where,

$\boldsymbol{\omega}$ - angular velocity of a fluid particle

Since the two dimensional flow field is assumed to be irrotational vorticity vanishes. Hence the irrotationality condition,

$$\nabla \times \vec{U} = 0 \tag{19}$$

(i.e. curl of the velocity vector field vanishes)

From the equation (19),

$$\left(\frac{\partial v}{\partial x} - \frac{\partial u}{\partial y}\right)\boldsymbol{k} = 0$$

where $\boldsymbol{k}$ is the unit vector along z axis.

Therefore,

$$\left(\frac{\partial v}{\partial x} - \frac{\partial u}{\partial y}\right) = 0 \tag{20}$$

3.2.1.2. <u>Complex potential</u>

By the equation (19), it can be shown that the integral,

$$\oint \vec{U}.dr = 0 \tag{21}$$

where,

$$dr = dx\boldsymbol{i} + dy\boldsymbol{j} \tag{22}$$

Therefore the integral is path independent. Then, by definition, the velocity vector field is a conservative vector field. And there exists a scalar potential function for the velocity vector field. It is called the velocity potential (ϕ) and can be represented by the equation (23).

$$\vec{U} = \nabla\phi \tag{23}$$

where, $\phi = \phi(x, y)$ and continuous in 2D space.

Further,

$$u = \frac{\partial \phi}{\partial x} \tag{24}$$

$$v = \frac{\partial \phi}{\partial y} \tag{25}$$

It can be shown by taking, the flux per unit length, into account that,

$$u = \frac{\partial \psi}{\partial y} \tag{26}$$

and

21

$$v = -\frac{\partial \psi}{\partial x} \qquad (27)$$

where, the stream function, $\psi = \psi(x, y)$ and continuous in 2D space.

Therefore, from equations (24), (25), (26) and (27),

$$\frac{\partial \phi}{\partial x} = \frac{\partial \psi}{\partial y} \qquad (28)$$

and

$$\frac{\partial \phi}{\partial y} = -\frac{\partial \psi}{\partial x} \qquad (29)$$

The equations (28) and (29) are called Cauchy-Riemann equations. Assuming that the partial derivatives of the equations (28) and (29) are continuous, then ϕ and ψ can be written such that,

$$W(z) = \phi(x, y) + i\psi(x, y)$$

where, $W(z)$ is an analytic (holomorphic) function of the complex variable $z \ (= x + iy)$ and i is the vector operator $\boldsymbol{k} \times$.

By partially differentiating the equations (28) and (29) w.r.t. x and y, it can be shown that,

$$\Delta\phi = 0 \qquad (30)$$
$$\Delta\psi = 0 \qquad (31)$$

Where Δ denotes the Laplacian operator (∇^2).

Therefore the stream function and the velocity potential satisfy the 2D Laplace equation. The solutions of the Laplace equations can be added to obtain new solutions. Therefore complex potentials of background flows can be added together to obtain new flow field which is the combined effect of the background flow fields.

In the current study, the complex potential associated with uniform flow and the complex potential associated with vortex motion are evaluated in a doubly connected domain.

3.2.1.3. <u>Boundary conditions</u>

Since the problem is to analyze the flow field around two aerofoil configurations which can be stationary/moving, two boundary conditions are to be satisfied. Those are as follows;

1. Far field boundary condition

2. Impermeability condition

3.2.1.3.1. <u>Far field boundary condition</u>

The velocity of the flow field should be equal to the free stream velocity as $|z| \to \infty$. Let the free stream velocity be U from negative to positive direction of the $x-$ axis.

Then the far field boundary condition,

$$\vec{U}\big|_{|z| \to \infty} = U \tag{32}$$

3.2.1.3.2. <u>Impermeability condition</u>

Let the boundaries of the aerofoils in the z - plane be ∂D_{zk} where $k = 1,2$ for boundaries of forward and rear aerofoils in tandem configuration and lower and upper aerofoils in unstaggered configuration respectively.
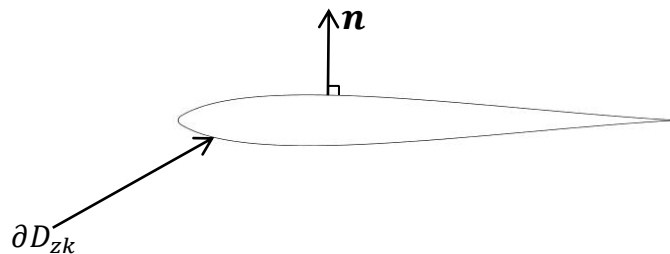
Figure 12: normal vector (**n**) and the boundary of an aerofoil

Since there is no flux through the boundary of the aerofoils the velocity at a point on the boundaries of the aerofoils should be equal to the velocity of the flow field at that point. Therefore,

$$\vec{U}.\boldsymbol{n} = \vec{u}.\boldsymbol{n} \tag{33}$$

where $\vec{u}$ is the velocity of a point on the boundary of the aerofoil.

When the aerofoils are stationary,

$$\vec{u} = 0$$

Therefore the impermeability condition on the boundaries of the aerofoils,

$$\vec{U}.\boldsymbol{n} = 0 \tag{34}$$

3.2.2. Uniform flow in doubly connected domains

3.2.2.1. Elliptic functions

3.2.2.1.1. Doubly periodic functions

Let ω_1 and ω_2 be two complex numbers whose ratio is also complex. A function $f(z)$ is called a doubly periodic function if,

$$f(z) = f(z + 2\omega_1) = f(z + 2\omega_2)$$

for all z for which $f(z)$ exists, $f(z)$ is called a doubly periodic function of z having periods $2\omega_1$ and $2\omega_2$.

A doubly periodic function that is analytic is called an elliptic function.

3.2.2.2. <u>Complex potential of uniform flow</u>

Complex potential associated with the doubly connected domain is formulated using elliptic functions since they are analytical except at isolated singularities at poles. Therefore elliptic functions naturally represent solutions to various flow patterns.

The annulus in ζ' - plane is further transformed into a rectangular slit domain in τ - plane using the mapping function (14).

τ - plane is the computational domain for the evaluation of the complex potential associated with the uniform flow in doubly connected domain.

The outer circle of the annulus in ζ' - plane is mapped into the line $\lambda = \lambda_2$ and the inner circle in the annulus is mapped into the line $\lambda = \lambda_1 = \log(q)$. The upper edge and the lower edge of the rectangle are $\mu = \pi$ and $\mu = -\pi$ respectively. Here, $\tau = \lambda + i\mu$.

The rectangle is defined as follows;

$$\lambda_1 \le Re(\tau) \le \lambda_2$$

and

$$-\pi \le Im(\tau) \le \pi$$

where,

$\lambda_1 = \log(r_1)$ and $\lambda_2 = \log(r_2)$, where r_1 and r_2 are the radii of the inner and outer circles of the annulus in ζ' - plane.

Here the origin of the τ - plane is inside the rectangle.

3.2.2.2.1. <u>Formulation of the complex potential of uniform flow</u>

The complex potential associated with the uniform flow, $w_{u\tau}(\tau)$ is evaluated first. Then the corresponding complex potential in ζ - plane is calculated using the mapping functions, (13) and (14) since further calculation is done in ζ - plane.

The complex velocity at z - plane is represented as follows,

$$\frac{dw_{u\tau}(\tau)}{dz} = \frac{dw_{u\tau}(\tau)}{d\tau}\frac{d\tau}{dz} \tag{35}$$

Where the complex velocity, $\frac{dw_{u\tau}(\tau)}{d\tau}$ at τ - plane should be a single valued analytical function of τ in the rectangular domain since the complex velocity $\frac{dw_{u\tau}(\tau)}{dz}$ at z - plane is a single valued analytical function of z. Therefore $w_{u\tau}(\tau)$ must possess a period of $2\pi i$. Also, it can be shown that the complex potential $w_{u\tau}(\tau)$ possesses a period of $2(\lambda_2 - \lambda_1)$.

Therefore $w_{u\tau}(\tau)$ is a doubly periodic function of τ having periods,

$$2\omega_1 = 2(\lambda_2 - \lambda_1) \tag{36}$$

and

$$2\omega_2 = 2\pi i \tag{37}$$

For further calculations a periodic rectangular domain is considered with following properties.

$$\lambda_1 \leq Re(\tau) \leq 2\lambda_2 + \lambda_1$$

and

$$-\pi \leq Im(\tau) \leq \pi$$

Therefore the complex velocity, $\frac{dw_{u\tau}(\tau)}{d\tau}$ has singularities at $\tau = 0$ and $\tau = 2\lambda_2$. Thus $\frac{dw_{u\tau}(\tau)}{d\tau}$ can be represented by the following elliptic function (38),

$$\frac{dw_{u\tau}(\tau)}{d\tau} = -2sUe^{-i\chi}\wp(\tau) + 2sUe^{i\chi}\wp(\tau - 2\lambda_1) + i\kappa \tag{38}$$

where s, κ are real constants, U is the free stream velocity at infinity, χ is the angle made by the free stream with the horizontal axis of z – plane and $\wp$ is the Weierstrass's elliptic function and it is defined as follows (39),

$$\wp(\tau) = \frac{1}{\tau^2} + \sum_{m,n=-\infty}^{+\infty\prime} \left[\frac{1}{(\tau - \Omega_{m,n})^2} - \frac{1}{\Omega_{m,n}^2} \right] \tag{39}$$

where,

$\Omega_{m,n} = 2n\omega_1 + 2m\omega_2$ for $m, n \in \mathbb{Z}$

The prime in the double series denotes the omission of the pair $(m,n) = (0,0)$. The Weierstrass's elliptic function converges absolutely and uniformly in the bounded rectangular domain.

By definition,

$$\wp(\tau) = -\frac{dZ(\tau)}{d\tau} \tag{40}$$

where $Z(\tau)$ is the Weierstrass's zeta function and defined as follows (41).

$$Z(\tau) = \frac{1}{\tau} + \sum_{m,n=-\infty}^{+\infty\prime} \left[\frac{1}{(\tau - \Omega_{m,n})} + \frac{1}{\Omega_{m,n}} + \frac{\tau}{\Omega_{m,n}^2} \right] \tag{41}$$

Equation (38) can be rearranged as equation (42),

$$\frac{dw_{u\tau}(\tau)}{d\tau} = 2sUe^{-i\chi}\frac{dZ(\tau)}{d\tau} - 2sUe^{i\chi}\frac{dZ(\tau - 2\lambda_1)}{d\tau} + i\kappa \tag{42}$$

By integrating the equation (42) with respect to τ,

$$w_{u\tau}(\tau) = -2sU(e^{-i\chi}Z(\tau) - e^{i\chi}Z(\tau - 2\lambda_1)) + i\kappa\tau + \kappa' \tag{43}$$

κ' is a constant that can be set to zero without affecting the solution.

By imposing Kutta condition at images of trailing edges on τ – plane where,

$$\frac{dw_{u\tau}(\tau)}{d\tau} = 0 \tag{44}$$

The constant κ is determined. Hence the above complex potential associated with uniform flow is unique.

Complex potential associated with the uniform flow in the ζ - plane can be obtained by using the mapping functions that transform τ - plane to ζ - plane. For further calculations the complex potential associated with the uniform flow should be expressed in terms of ζ since the main computational domain is taken to be the ζ - plane.

3.2.3. Modeling free shear layers

Free shear layers of the flow field is modeled by using point vortices.

3.2.3.1. Point vortex

Complex potential associated with a point vortex with a circulation of Γ is as follows;

$$w = -\frac{i\Gamma}{2\pi}\ln(z - z_0) \tag{45}$$

where,

Γ - circulation/strength of the point vortex

z - complex variable in z - plane

z_0 - position of the point vortex at z - plane

3.2.4. <u>Vortex Motion in doubly connected domain</u>

Instantaneous complex potential of the vortex motion in doubly connected domain is evaluated using the method introduced in [13]. The complex potential associated with a point vortex of unit circulation at point γ inducing -1 circulation around the inner circle j and null circulations around other inner and outer circles in the annulus in ζ − plane is given by the modified Green's function,

$$G_j(\zeta,\gamma) = -\frac{i}{2\pi}\ln\left(\frac{\omega(\zeta,\gamma)}{|\gamma|\omega(\zeta,\theta_j(\bar{\gamma}^{-1}))}\right) \tag{46}$$

where,

$$\theta_k(\zeta) = \delta_k + \frac{q_k^2\zeta}{1-\bar{\delta}_k\zeta} \tag{47}$$

$\theta_k(\zeta)$ - generator associated with k^{th} inner circle in ζ - plane

k - number of generators (number of inner circles $(= 1)$)

q_k - radius of the kth inner circle

δ_k - center of the kth inner circle

For $j = 0$,

$$G_0(\zeta,\gamma) = -\frac{i}{2\pi}\ln\left(\frac{\omega(\zeta,\gamma)}{|\gamma|\omega(\zeta,\bar{\gamma}^{-1})}\right) \tag{48}$$

$G_0(\zeta,\gamma)$ is the complex potential due to vortex at point γ in ζ plane which induces -1 circulation around the outer circle and null circulation around inner circle.

Since only one generator is associated with doubly connected domain,

$$\theta_1(\zeta) = q^2\zeta \tag{49}$$

Therefore,

For $j = 1$,

$$G_1(\zeta, \gamma) = -\frac{i}{2\pi} \ln \left(\frac{\omega(\zeta, \gamma)}{|\gamma| \omega(\zeta, q^2 \bar{\gamma}^{-1})} \right) \tag{50}$$

$G_1(\zeta, \gamma)$ is the complex potential due to vortex at point γ in ζ plane which induces -1 circulation around the inner circle and null circulation around outer circle.

As mentioned by [13] circulations around the circles in ζ - plane can be specified by simply multiplying the relevant Green's function by the required value of circulation.

3.2.4.1. <u>Computing Schottky Klein prime function</u>

To obtain the modified Green's function for the vortex motion in doubly connected domain, computation of Schottky Klein prime function is needed. First set of M Mobius maps [43], [46] should be defined for each inner circle assuming there are M inner circles in the computational domain D_ζ in ζ - plane (in fact there is only one inner circle in the domain under consideration since the problem is doubly connected).

Let

$$\theta_j(\zeta) = \frac{a_j \zeta + b_j}{c_j \zeta + d_j} \tag{51}$$

for $j = 1,2, \ldots, M$

where,

$$a_j = q_j - \frac{|\delta_j|^2}{q_j}$$

30

$$b_j = \frac{\delta_j}{q_j}$$

$$c_j = -\frac{\bar{\delta}_j}{q_j}$$

$$d_j = \frac{1}{q_j}$$

Here, q_j and δ_j are radius and center of the jth circle respectively. The inverse of a Mobius map also becomes a Mobius map. Therefore M additional maps can be generated considering the inverse maps. Also, composition of a Mobius map with another Mobius map results another new Mobius map. Therefore composition of M Mobius maps with their M inverse maps generates infinite number of additional Mobius maps. The infinite set of Mobius maps can be categorized according to their level while level 1 being the basic Mobius maps and their inverses. To compute the SK function all these Mobius maps are needed excluding inverse maps and the compositions that reduces to a lower level map or reduces to identity map (Schottky Group is defined with all the maps). Therefore the categorization of the maps is as follows (subset of Schottky Group, the set θ).

Level 1 maps: (basic maps or generators)

$\theta_1, \theta_2, \ldots \ldots \ldots \ldots, \theta_M$

Level 2 maps: (combinations of composite functions)

$\theta_1^2, \theta_1\theta_2, \theta_1\theta_3, \ldots.., \theta_1\theta_M, \theta_2\theta_1, \theta_2^2, \ldots.., \theta_M\theta_{M-1}, \theta_M^2$

Level 3 maps:

All the composite functions of any three basic maps

All the higher level maps are defined in a similar manner.

The Schottky Klein prime function is defined as in equation (52),

$$\omega(\zeta, \gamma) = (\zeta - \gamma)\omega'(\zeta, \gamma) \tag{52}$$

Where,

$$\omega'(\zeta, \gamma) = \prod_{\theta_k \in \theta} \frac{(\theta_k(\zeta) - \gamma)(\theta_k(\gamma) - \zeta)}{(\theta_k(\zeta) - \zeta)(\theta_k(\gamma) - \gamma)} \tag{53}$$

ζ, γ - complex variables

θ - a subset of Schottky group

θ_k - elements in the subset of θ

When evaluating the infinite formula, the subset of the Schottky group is selected such that the elements up to some level are included.

Since the problem is doubly connected there's only one generator (one basic map) associated with the problem [44]. Therefore only the case when $j = 1$ is considered. When $j = 1$, the inner circle in the annulus should be considered. The radius and the center of the inner circle are q and 0 respectively. Therefore, $\delta_1 = 0$ and $q_1 = q$.

From equation (51) the basic Mobius map becomes the equation (49),

$$\theta_1(\zeta) = q^2 \zeta$$

The infinite number of maps are easily computed from the equation (49).

Level 1 maps:

$\theta_1(\zeta) = q^2 \zeta$

Level 2 maps:

$$\theta_1\big(\theta_1(\zeta)\big) = q^4\zeta$$

Level 3 maps:

$$\theta_1\left(\theta_1\big(\theta_1(\zeta)\big)\right) = q^6\zeta$$

Level k maps:

$$\theta_1\dots\left(\theta_1..\big(\theta_1(\zeta)\big)\right) = q^{2k}\zeta$$

To compute the modified Green's functions, (48), (50), $\omega(\zeta,\gamma)$ and $\omega(\zeta,\theta_1(\bar{\gamma}^{-1}))$ should be calculated. By incorporating infinite number of level maps $\omega(\zeta,\gamma)$ and $\omega(\zeta,\theta_1(\bar{\gamma}^{-1}))$ can be written as follows,

$$\omega(\zeta,\gamma) = (\zeta - \gamma)\prod_{k=1}^{\infty}\frac{(1 - q^{2k}\zeta\gamma^{-1})(1 - q^{2k}\zeta^{-1}\gamma)}{(1 - q^{2k})^2} \tag{54}$$

$$\omega(\zeta,\theta_1(\bar{\gamma}^{-1})) = \left(\zeta - \frac{q^2}{\bar{\gamma}}\right)\prod_{k=1}^{\infty}\frac{(1 - q^{2k-2}\zeta\bar{\gamma})(1 - q^{2k+2}(\zeta\bar{\gamma})^{-1})}{(1 - q^{2k})^2} \tag{55}$$

3.3. Modeling the flow field

3.3.1. Vortex shedding mechanism

Initially two vortices are placed near the trailing edges as shown in figure 13, 0.001 distance downstream which is in the range of values recommended in the literature [47].
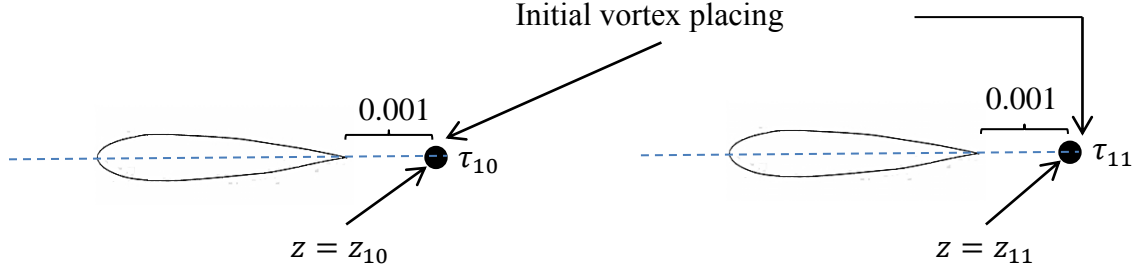
Figure 13: initial vortex placement: tandem aerofoil configuration

3.3.2. <u>Calculating strengths of the initial vortices</u>

Strengths of the initial vortices are found by incorporating the Kutta condition [42]. Since the aerofoils are mapped into two circles, the derivative $\frac{d\zeta}{dz}$ is singular at trailing edges (due to the sharp edges). Then, for the velocity at z - plane $(\frac{dW}{dz})$ to be finite, the velocity at the corresponding points in ζ - plane $(\frac{dW}{d\zeta})$ should be zero.

Therefore,

$$\frac{dW(\zeta)}{d\zeta}\bigg|_{\substack{\zeta=t_0 \\ \zeta=t_1}} = 0 \tag{56}$$

t_0 - trailing edge position of the front aerofoil in ζ - plane

t_1 - trailing edge position of the rear aerofoil in ζ - plane

Let $z = z_{10}$ maps $\zeta = \gamma_{10}$ and $z = z_{11}$ maps $\zeta = \gamma_{11}$,

Since,

$W(\zeta) = W_v(\zeta) + W_u(\zeta),$

34

$$\frac{d(W_v(\zeta) + W_u(\zeta))}{d\zeta}\Bigg|_{\substack{\zeta=t_0 \\ \zeta=t_1}} = 0$$

$$\frac{d(\tau_{10}G_0(\zeta,\gamma_{10}) + \tau_{11}G_1(\zeta,\gamma_{11}) + W_u)}{d\zeta}\Bigg|_{\substack{\zeta=t_0 \\ \zeta=t_1}} = 0$$

$$\left[\tau_{10}\frac{dG_0(\zeta,\gamma_{10})}{d\zeta} + \tau_{11}\frac{dG_1(\zeta,\gamma_{11})}{d\zeta} + \frac{dW_u(\zeta)}{d\zeta}\right]\Bigg|_{\substack{\zeta=t_0 \\ \zeta=t_1}} = 0$$

$$\begin{bmatrix} \tau_{10} \\ \tau_{11} \end{bmatrix} = - \begin{bmatrix} \dfrac{dG_0(\zeta,\gamma_{10})}{d\zeta}\Big|_{\zeta=t_0} & \dfrac{dG_1(\zeta,\gamma_{11})}{d\zeta}\Big|_{\zeta=t_0} \\ \dfrac{dG_0(\zeta,\gamma_{10})}{d\zeta}\Big|_{\zeta=t_1} & \dfrac{dG_1(\zeta,\gamma_{11})}{d\zeta}\Big|_{\zeta=t_1} \end{bmatrix}^{-1} \begin{bmatrix} \dfrac{dW_u(\zeta)}{d\zeta}\Big|_{\zeta=t_0} \\ \dfrac{dW_u(\zeta)}{d\zeta}\Big|_{\zeta=t_1} \end{bmatrix}$$

$$\tau = -V^{-1}F \qquad\qquad (57)$$

where the matrices,

$$\tau = \begin{bmatrix} \tau_{10} \\ \tau_{11} \end{bmatrix}, V = \begin{bmatrix} \dfrac{dG_0(\zeta,\gamma_{10})}{d\zeta}\Big|_{\zeta=t_0} & \dfrac{dG_1(\zeta,\gamma_{11})}{d\zeta}\Big|_{\zeta=t_0} \\ \dfrac{dG_0(\zeta,\gamma_{10})}{d\zeta}\Big|_{\zeta=t_1} & \dfrac{dG_1(\zeta,\gamma_{11})}{d\zeta}\Big|_{\zeta=t_1} \end{bmatrix} \text{ and } F = \begin{bmatrix} \dfrac{dW_u(\zeta)}{d\zeta}\Big|_{\zeta=t_0} \\ \dfrac{dW_u(\zeta)}{d\zeta}\Big|_{\zeta=t_1} \end{bmatrix}$$

3.3.3. <u>Calculating velocities of the initial vortices</u>

To find the velocity at initial vortex points, individual contributions of induced velocities are taken into account.

$$\begin{array}{c} \text{Velocity at a} \\ \text{vortex point} \end{array} = \begin{array}{c} \text{Velocity induced by} \\ \text{free stream at the} \\ \text{vortex point} \end{array} + \begin{array}{c} \text{Velocity induced by} \\ \text{other vortex at the} \\ \text{vortex point} \end{array}$$

Hence the velocities at the vortex points are calculated using Routh's Rule [38],

$$\bar{V}_l = \frac{dW_l(\zeta)}{d\zeta}\frac{d\zeta}{dz} - \frac{i\tau_l}{4\pi}\frac{\frac{d^2\zeta}{dz^2}}{\frac{d\zeta}{dz}} \tag{58}$$

where,

$\bar{V}_l$ is the complex conjugate velocity at vortex point z, having a vortex with a circulation of τ_l and,

$$W_l(\zeta) = W_u(\zeta) + W_v(\zeta) - \left(-\frac{i\tau_l}{2\pi}\ln(\zeta - \gamma_l)\right) \tag{59}$$

γ_l is the point in ζ plane that maps the vortex point in z - plane.

Here the complex potential associated with the vortex at the point corresponding to the point γ_l in z - plane is removed from the complex potential of the flow field.

Using the equation (58),

Complex conjugate velocities at the vortex points near the front and rear aerofoils,

$$\bar{V}_{1j} = \left[\frac{dW_{1j}(\zeta)}{d\zeta}\frac{d\zeta}{dz} - \frac{i\tau_{1j}}{4\pi}\frac{\frac{d^2\zeta}{dz^2}}{\frac{d\zeta}{dz}}\right]\Bigg|_{\substack{z=z_{1j}\\ \zeta=\gamma_{1j}}}$$

where,

$$W_{1j}(\zeta) = \left[W_u(\zeta) + W_v(\zeta) - \left(-\frac{i\tau_{10}}{2\pi}\ln(\zeta - \gamma_{1j})\right)\right]\Bigg|_{\zeta=\gamma_{1j}}$$

$j = 0,1$ ('0' for front aerofoil and '1' for rear aerofoil)

$\bar{V}_{1j}$ - Complex conjugate velocities at the vortex points

z_{1j} - Vortex points near the front/rear aerofoils

γ_{1j} - Points in ζ – plane that maps the points $z = z_{1j}$ in z - plane

τ_{1j} - Strengths of the vortice at points $z = z_{1j}$

After finding out the initial velocities, the vortices are moved by a time step, Δt. Depending on the application values for Δt were taken in the range $0.001 - 0.02$.

Distance moved by the initial vortices at the time step Δt is taken as follows;

$$\Delta z_{1j} = \bar{V}_{1j}.\Delta t$$

Then another two vortices are introduced to the flow field as the Kutta condition violates. Then these newly added vortices are moved after calculating the strengths and the velocities together with the other two vortices. This process is repeated to model the free shear layers of the flow field.

3.3.4. <u>Generalized formulation for strengths and velocities</u>

Let there be N vortices in the flow field. Calculation of the strengths of the newly added vortices and the velocities of the vortex points in the flow field are as shown in figure 14.
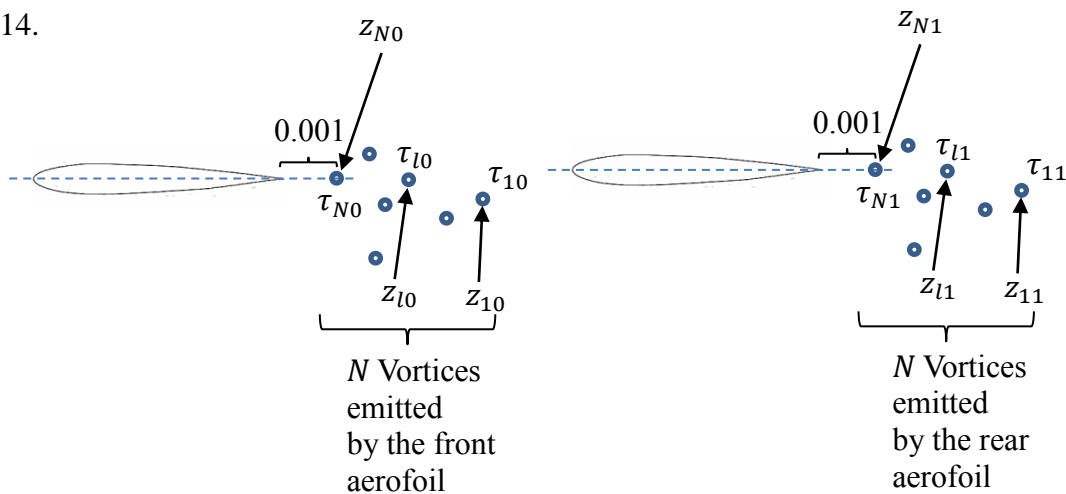

Figure 14: Aerofoils in tandem configuration with vortex production

Where z_{1j} maps γ_{1j} in ζ - plane, z_{lj} maps γ_{lj} in ζ - plane and z_{Nj} maps γ_{Nj} in ζ - plane for $j = 0,1$.

By Kutta condition,

At the trailing edges,

$$\left. \frac{d(W_v(\zeta) + W_u(\zeta))}{d\zeta} \right|_{\substack{\zeta=t_0 \\ \zeta=t_1}} = 0$$

$$W_v = \sum_{l=1}^{N} \tau_{l0} G_0(\zeta, \gamma_{l0}) + \sum_{l=1}^{N} \tau_{l1} G_1(\zeta, \gamma_{l1})$$

After solving for τ_{N0} and τ_{N1},

$$\tau = -V^{-1}F$$

Where,

$$\tau = \begin{bmatrix} \tau_{N0} \\ \tau_{N1} \end{bmatrix}$$

$$V = \begin{bmatrix} \left. \dfrac{dG_0(\zeta, \gamma_{N0})}{d\zeta} \right|_{\zeta=t_0} & \left. \dfrac{dG_1(\zeta, \gamma_{N1})}{d\zeta} \right|_{\zeta=t_0} \\ \left. \dfrac{dG_0(\zeta, \gamma_{N0})}{d\zeta} \right|_{\zeta=t_1} & \left. \dfrac{dG_1(\zeta, \gamma_{N1})}{d\zeta} \right|_{\zeta=t_1} \end{bmatrix}$$

$$F = \begin{bmatrix} \left. \left(\dfrac{d(W_u)}{d\zeta} + \sum_{l=1}^{N-1} \tau_{l0} G_0(\zeta, \gamma_{l0}) + \sum_{l=1}^{N-1} \tau_{l1} G_1(\zeta, \gamma_{l1}) \right) \right|_{\zeta=t_0} \\ \left. \left(\dfrac{d(W_u)}{d\zeta} + \sum_{l=1}^{N-1} \tau_{l0} G_0(\zeta, \gamma_{l0}) + \sum_{l=1}^{N-1} \tau_{l1} G_1(\zeta, \gamma_{l1}) \right) \right|_{\zeta=t_1} \end{bmatrix}$$

Velocity of a vortex point can be obtained by using the Routh's rule (58).

3.4. Evaluating forces on the aerofoils

3.4.1. Formulation of the governing equation

Forces per unit span on the aerofoils can be calculated by integrating the pressure on the boundaries with respect to arc length of the boundary.

Then the vector form of the force per unit length on the aerofoils,

$$\boldsymbol{F}^{[k]} = -\oint_{\partial D_{zk}} P\boldsymbol{n}\, dl \tag{60}$$

$k = 1,2$

$\boldsymbol{n}$ - unit normal vector of the boundary

dl - integral path along the boundary (arc length)

P - pressure on the boundary

Unsteady Bernoulli's equation along a streamline,

$$-\frac{P}{\rho} = \frac{\partial \phi}{\partial t} + \frac{1}{2}|\vec{U}|^2 \tag{61}$$

where ρ is the density of the fluid.

From (60) and (61),

$$\boldsymbol{F}^{[k]} = \rho.\oint_{\partial D_{zk}} \left(\frac{\partial \phi}{\partial t} + \frac{1}{2}|\vec{U}|^2\right)\boldsymbol{n}\, dl$$

Complex form of the equation can be written as follows;

$$F^{[k]} = F_x^{[k]} - iF_y^{[k]} = -i\oint_{\partial D_{zk}} Pd\bar{z}$$

where $\bar{z}$ is the complex conjugate of the complex variable, z and $F^{[k]}$ is the complex force on the aerofoils for $k = 1, 2$.

$$F^{[k]} = F_x^{[k]} - iF_y^{[k]} = -i\rho \oint_{\partial D_{zk}} \left(\frac{\partial \phi}{\partial t} + \frac{1}{2} |\vec{U}|^2 \right) d\bar{z}$$

Since,

$$|\vec{U}|^2 = \frac{dw(z)}{dz} \overline{\left(\frac{dw(z)}{dz} \right)} = \frac{dw(z)}{dz} \frac{dw(z)}{d\bar{z}}$$

where 'bar' denotes the complex conjugate and since boundaries are constant streamlines, then along a streamline, $d\psi = 0$. Hence $w(z) = \bar{w}(z)$.

Then,

$$F^{[k]} = F_x^{[k]} - iF_y^{[k]} = -i\rho \oint_{\partial D_{zk}} \left(\frac{\partial \phi}{\partial t} + \frac{1}{2} \frac{dw(z)}{dz} \frac{dw(z)}{d\bar{z}} \right) d\bar{z}$$

$$F^{[k]} = F_x^{[k]} - iF_y^{[k]} = -\frac{i\rho}{2} \oint_{\partial D_{zk}} \left(\frac{dw(z)}{dz} \right)^2 dz - i.\rho \oint_{\partial D_{zk}} \overline{\left(\frac{\partial \phi}{\partial t} \right)} dz \qquad (62)$$

The above equation (62) is called the unsteady Blasius equation. The equation has a steady part and an unsteady part.

Steady part:

$$-\frac{i\rho}{2} \oint_{\partial D_{zk}} \left(\frac{dw(z)}{dz} \right)^2 dz$$

Unsteady part:

$$-i.\rho \oint_{\partial D_{zk}} \overline{\left(\frac{\partial \phi}{\partial t} \right)} dz$$

Since the computational domain is the annulus in ζ - plane the equation (62) is represented by the variable ζ in ζ - plane.

By chain rule,

$$\frac{dw(z)}{dz} = \frac{dw(z)}{d\zeta}\frac{d\zeta}{dz}$$

also,

$$w(z) = W(\zeta)$$

Then the equation (62) can be rearranged as follows,

$$F^{[k]} = F_x^{[k]} - iF_y^{[k]} = -\frac{i\rho}{2}\oint_{\partial D_{\zeta k}}\left(\frac{dW(\zeta)}{d\zeta}\right)^2\left(\frac{d\zeta}{dz}\right)d\zeta - i.\rho\oint_{\partial D_{zk}}\overline{\left(\frac{\partial\phi}{\partial t}\right)dz}$$

Here $\partial D_{\zeta k}$ (for $k = 1,2$) are the outer and inner boundaries on the annulus in ζ - plane respectively.

Since the stream function is an instantaneous constant on the boundaries, $\psi = c(t)$, where $c(t)$ is an instantaneous constant.

Since $w(z) = \phi + i\psi$

Taking the conjugate,

$$\overline{w(z)} = \phi - i\psi$$

differentiating partially with respect to t,

$$\frac{\partial\overline{w(z)}}{\partial t} = \frac{\partial\phi}{\partial t} - i\frac{\partial\psi}{\partial t} \tag{63}$$

on the boundaries,

$$\frac{\partial\psi}{\partial t} = c'(t)$$

'prime' denotes the derivative.

From the equation (63),

$$\frac{\partial \overline{w(z)}}{\partial t} = \frac{\partial \phi}{\partial t} - ic'(t) \tag{64}$$

Using the above equations (63) and (64), the unsteady part of the equation (62) can be written as follows,

$$-i.\rho \oint_{\partial D_{zk}} \overline{\left(\frac{\partial \phi}{\partial t}\right)} dz = -i.\rho \oint_{\partial D_{zk}} \overline{\left(\frac{\partial \overline{w(z)}}{\partial t} + ic'(t)\right)} dz = -i.\rho \frac{\partial}{\partial t} \oint_{\partial D_{\zeta k}} W(\zeta) \overline{\left(\frac{dz}{d\zeta}\right)} d\zeta$$

Then the equation (62) can be rearranged as follows,

$$F^{[k]} = F_x^{[k]} - iF_y^{[k]}$$

$$= -\frac{i\rho}{2} \oint_{\partial D_{\zeta k}} \left(\frac{dW(\zeta)}{d\zeta}\right)^2 \left(\frac{d\zeta}{dz}\right) d\zeta - i.\rho \frac{\partial}{\partial t} \oint_{\partial D_{\zeta k}} W(\zeta) \overline{\left(\frac{dz}{d\zeta}\right)} d\zeta \tag{65}$$

3.4.2. Numerical Quadrature

Equation (65) cannot be solved using analytical methods due to its highly non-linear nature and as the complex potentials are evaluated instantaneously, time dependence of the complex potential is not obtained. Therefore a numerical quadrature is incorporated to solve the equation.

The steady part and the unsteady part of the Blasius equation (65) are considered separately. Both the integrands of the integrals in the steady and the unsteady parts of the equation are analytical functions and integrals are taken over circles in the complex plane. Therefore the best way to evaluate the integrals is to incorporate trapezoidal rule

due to its accuracy when dealing with integrals of periodic analytic functions over a periodic interval.

When considering the unsteady part of the equation (65) there is a partial derivative with respect to time associated with it. It cannot be solved since the time dependence of the complex potential is not evaluated. Therefore the partial time derivative is numerically solved using a finite difference method.

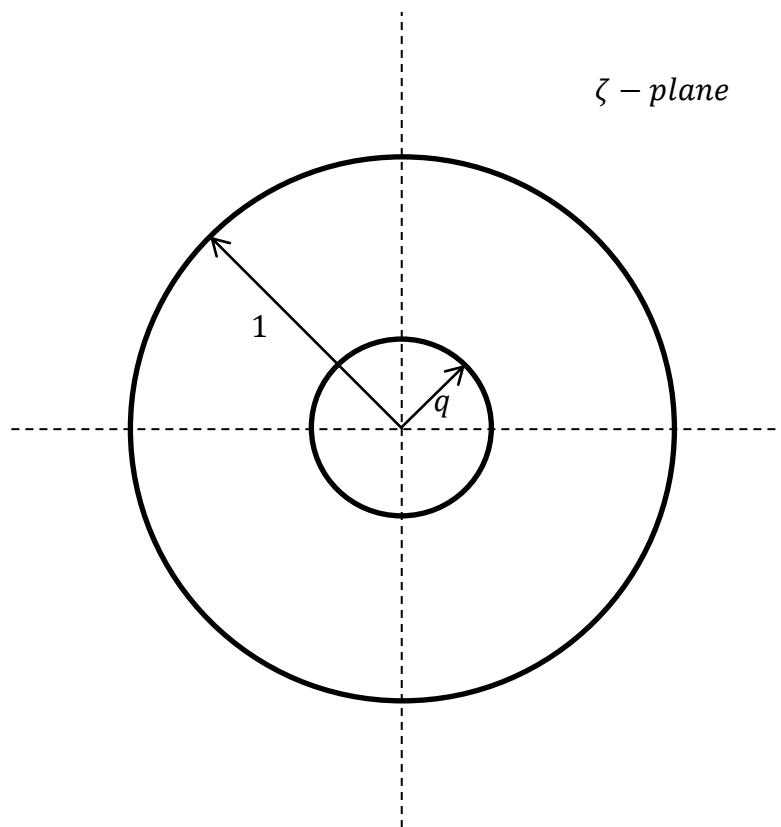### 3.4.2.1. <u>Trapezoidal rule</u>

Figure 15: computational domain (Annulus) in ζ - plane

Let the integrands of the integrals in steady and unsteady parts of the equation (65) be $f_{sk}(\zeta)$ and $f_{uk}(\zeta)$ respectively.
Therefore,

$$f_{sk}(\zeta) = -\frac{i\rho}{2}\left(\frac{dW(\zeta)}{d\zeta}\right)^2\left(\frac{d\zeta}{dz}\right) \tag{66}$$

and

$$f_{uk}(\zeta) = i\rho W(\zeta)\left(\frac{dz}{d\zeta}\right) \tag{67}$$

To implement the trapezoidal rule the angle at the centers of the circles are divided into equal N parts. Also N points in each circle are selected.
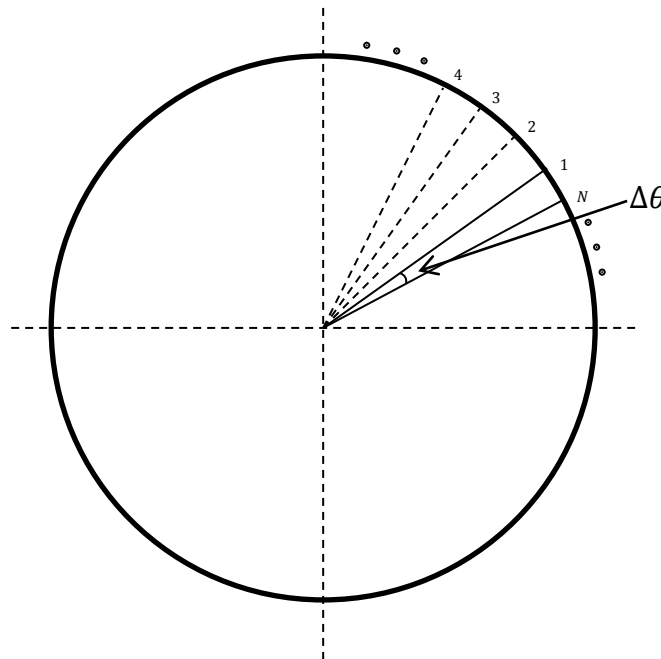

Figure 16: discretizing the circle to equally spaced angles

The angle,

$$\Delta\theta = \frac{2\pi}{N}$$

N has to be selected so that the error associated with the numerical quadrature is minimized. It is selected to be $N = 5000$.

Let,

$$\theta_n = n\Delta\theta, \quad for\ n = 1,2,\dots,N$$

Values of ζ on the circles can be represented as follows,

$$\zeta = r_k e^{i\theta_n}$$

$$\zeta = r_k e^{i\left(\frac{2\pi}{N}\right)n}, \qquad for\ k = 1,2$$

Note that $r_1 = 1$ and $r_2 = q$.

Then the integrals of the Blasius equation are evaluated as follows,

3.4.2.1.1. The steady integral of the Blasius equation

$$I_{sk} = \oint_{\partial D_{\zeta k}} -\frac{i\rho}{2}\left(\frac{dW(\zeta)}{d\zeta}\right)^2 \left(\frac{d\zeta}{dz}\right) d\zeta$$

By trapezoidal rule,

$$I_{sk} \approx \sum_{n=1}^{N} f_{sk}\left(r_k e^{i\left(\frac{2\pi}{N}\right)n}\right), for\ k = 1,2$$

Here, when evaluating the above integral, the circles are slightly extended to the fluid domain at the corresponding trailing edge positions in the ζ domain to avoid the trailing edge singularity associated with the mapping function when mapping sharp edges.

3.4.2.1.2. The integral of the unsteady part

$$I_{uk} = -i.\rho\overline{\frac{\partial}{\partial t}\oint_{\partial D_{\zeta k}} W(\zeta)\left(\frac{dz}{d\zeta}\right) d\zeta}$$

The integral is evaluated by trapezoidal rule,

$$\oint_{\partial D_{\zeta_k}} W(\zeta) \left(\frac{dz}{d\zeta}\right) d\zeta \approx \sum_{n=1}^{N} f_{uk} \left(r_k e^{i\left(\frac{2\pi}{N}\right)n}\right), for\ k = 1,2$$

The above integrals are evaluated at every time step using the trapezoidal rule as shown.

3.4.2.1.3. Initial conditions

Initially two vortices are placed downstream of the aerofoils and the strengths of the initial vortices are calculated using Kutta condition as mentioned in section 3.3.2.. The complex potential at this initial state is evaluated around the two circles and also the derivatives of the complex potentials with respect to the variable ζ are evaluated on the two circles. This corresponds to the evaluation of complex velocities at the selected points on the two circles (N points on each circle). Initial value of the equation (63) has to be found to evaluate the unsteady part of the Blasius equation.

Initial conditions;

$$f_{uk}(\zeta)|_{t=0} = i\rho W(\zeta)|_{t=0} \left(\frac{dz}{d\zeta}\right)$$

where,

$$W(\zeta)|_{t=0} = W_u(\zeta)|_{t=0} + \tau_{10} \frac{dG_0(\zeta, \gamma_{10})}{d\zeta} + \tau_{11} \frac{dG_1(\zeta, \gamma_{11})}{d\zeta}$$

$W(\zeta)|_{t=0}$ is evaluated around both circles.

3.4.2.2. Evaluating unsteady part of the Blasius equation

A finite difference method is used to evaluate the unsteady part of the Blasius equation at each time step. The time step is taken as the time step taken to shed vortices which varies from 0.001 - 0.02, depending on the application.

$$I_{uk}|_j = -i \cdot \rho \frac{\partial}{\partial t} \overline{\oint_{\partial D_{\zeta k}} W(\zeta)|_J \left(\frac{dz}{d\zeta}\right) d\zeta}$$

where, $j = 0, 1, 2, \ldots$

$j = 0$ corresponds to the initial condition (when $t = 0$).

The unsteady part can be rearranged as follows,

$$I_{uk}|_j = -i \cdot \frac{\partial}{\partial t} \overline{\oint_{\partial D_{\zeta k}} \rho W(\zeta)|_J \left(\frac{dz}{d\zeta}\right) d\zeta}$$

Let,

$$F_j = -i \cdot \overline{\oint_{\partial D_{\zeta k}} \rho W(\zeta)|_J \left(\frac{dz}{d\zeta}\right) d\zeta}$$

Then the finite difference scheme is,

$$I_{uk}|_{j+1} = \frac{F_{j+1} - F_j}{\Delta t}$$

where the time step, Δt varies from 0.001 - 0.02 depending on the application.

I_{sk} and I_{uk} are evaluated at every time step and hence the complex forces on the aerofoils are obtained. Then x and y components of the force are obtained by considering real and imaginary parts of the complex force.

$$F_x^{[k]} = real\left(F^{[k]}\right)$$

$$F_y^{[k]} = -imag\left(F^{[k]}\right)$$

The lift coefficient and the drag coefficient are calculated by using equations (68) and (69),

$$C_L = \frac{F_y^{[k]}}{0.5\rho U^2 c} \tag{68}$$

$$C_D = \frac{F_x^{[k]}}{0.5\rho U^2 c} \tag{69}$$

where ρ is the density of the air and c is the chord length of the identical aerofoils.

4. RESULTS AND DISCUSSION

4.1. Validation

4.1.1. Single plunging aerofoil

The flow pattern for the single aerofoil in plunging motion is obtained by separating aerofoils 50 times the chord length as shown in the figure 19. The reduced frequency is taken to be 3. And the plunge amplitude is taken to be 0.2 units while the non-dimensionalized time step being at 0.007. These values are taken to validate the current developed model.

Reduced frequency,

$$k = \frac{\omega c}{U_\infty} \tag{70}$$

Non-dimensionalized time,

$$\bar{t} = \frac{tU_\infty}{c} \tag{71}$$

The separation of the aerofoils leads to the assumption of the effect of the vortices emitted by each aerofoil on the other aerofoil should be negligible. Hence a flow pattern with a perfect qualitative agreement with the experimental data obtained by Jones et al. [21] for a single plunging aerofoil is obtained using the model developed. The wake structures obtained by Jones et al. [21] using inviscid panel code and using water tunnel experimental procedures are shown in the figure 17. The wake pattern obtained by using the current model is shown in the figure 18. It can be concluded that the wake formation of the plunging aerofoil is essentially an inviscid phenomena due to the excellent qualitative agreement with the inviscid wake structure and the experimental wake structure.
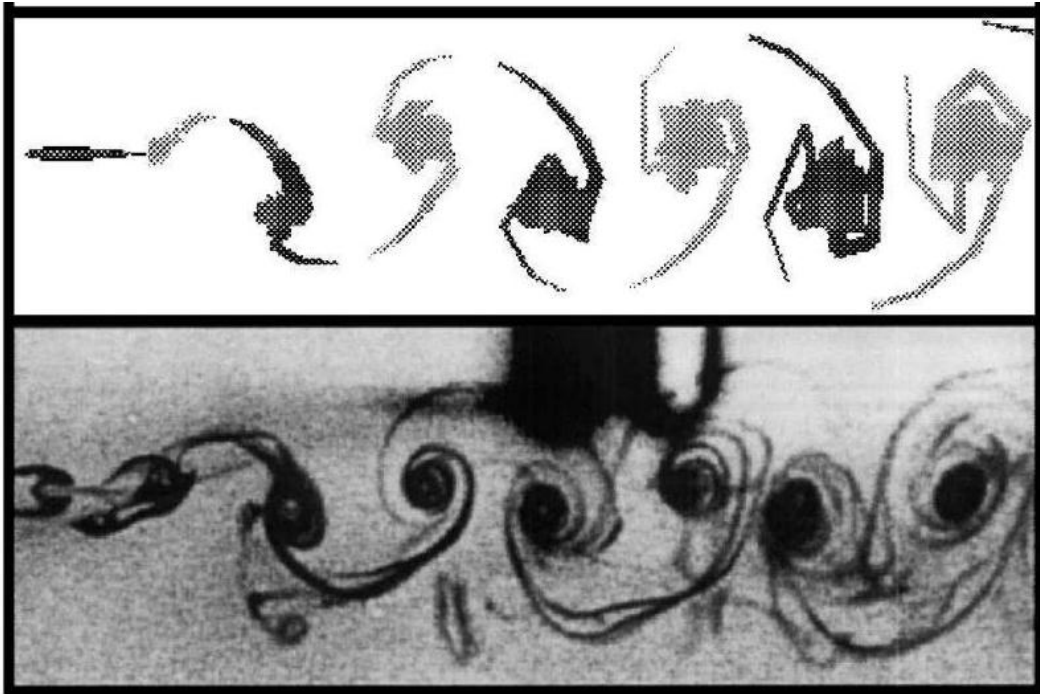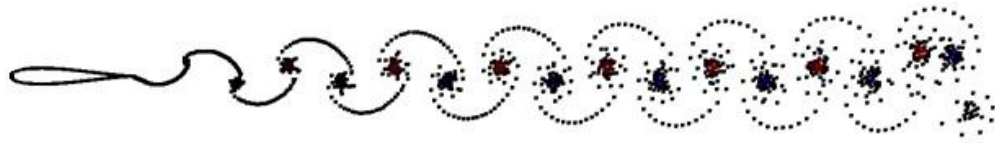
Figure 17: Result obtained by Jones et al. [21]
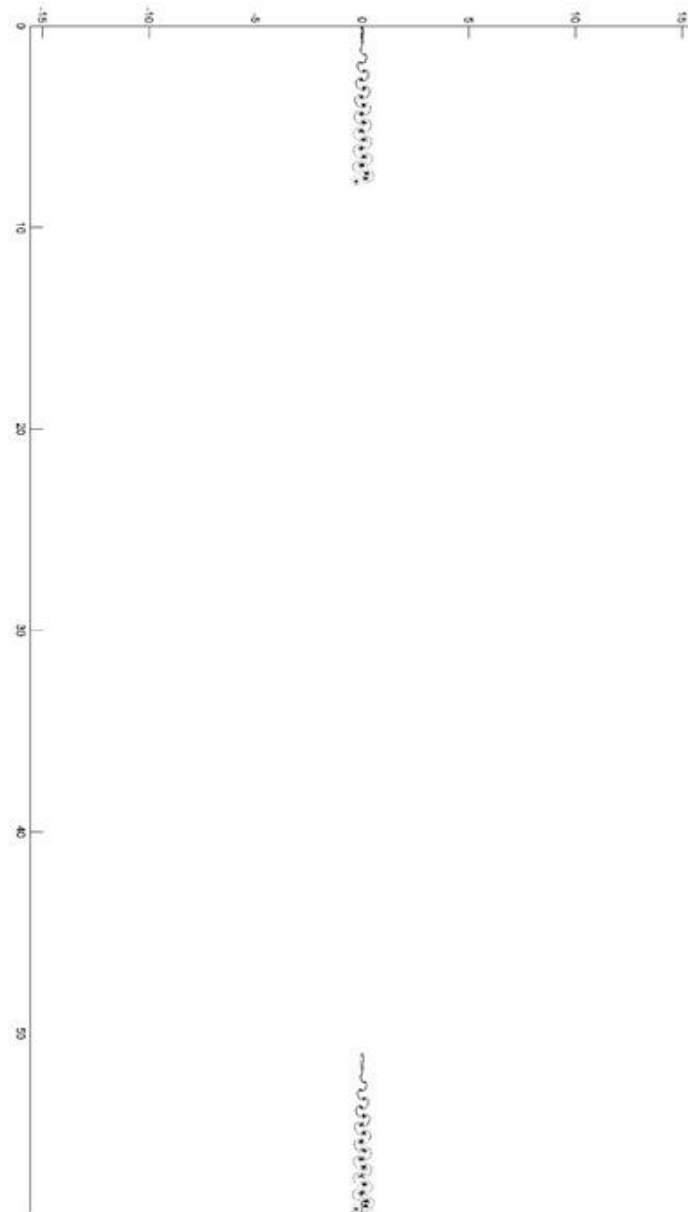

Figure 18: Result obtained by the model developed

Figure 19: plunging aerofoils at 50c distance apart

For the validation of the model developed for predicting unsteady forces, plunging aerofoils at distance 50c apart are considered. The reduced frequency, non-dimensionalized time step and plunging amplitude are taken to be 17, 0.015 and 0.018 respectively. Then the harmonic unsteady lift coefficient is calculated using the developed model. Finally a graph is plotted for the harmonic lift coefficient vs. the product of reduced frequency and time. An excellent qualitative agreement is observed with the data obtained by Yao et al. [24] as shown in the figure 20.
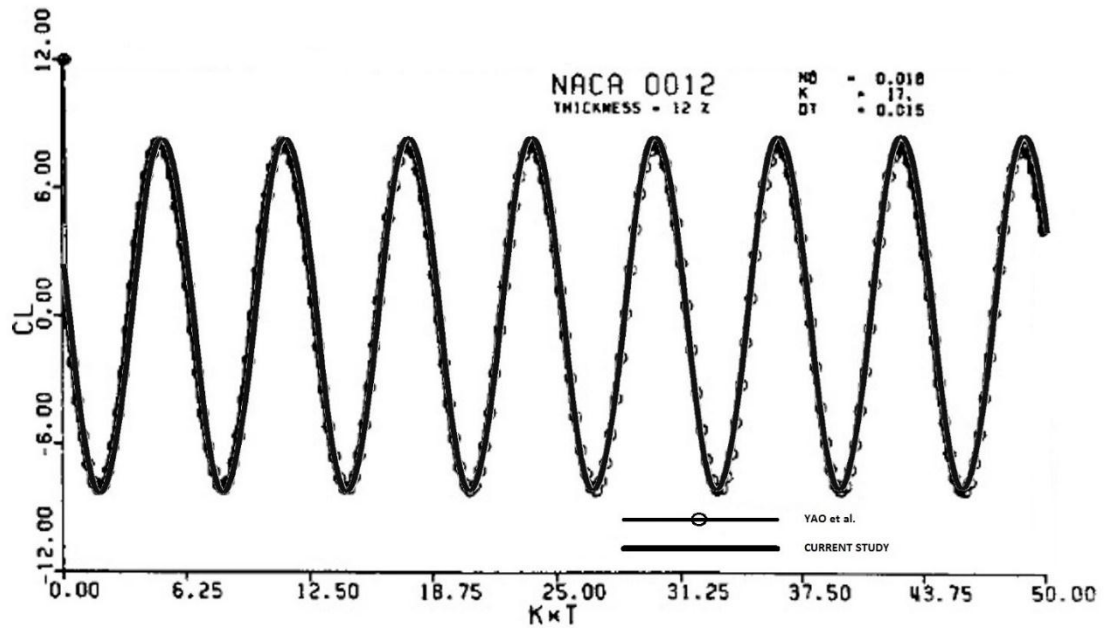

Figure 20: harmonic lift compared with data by Yao et. al [24]

4.1.2. <u>Tandem aerofoils</u>

Three tandem aerofoil configurations are selected for validation. Gap is varied in three configurations while the horizontal gap and the decalage to be taken as 0.5c and 0 respectively. The gaps in the three configurations are selected to be 0.2c, 0 and -0.2c. The flow pattern and the unsteady lift coefficient are evaluated for each case and compared with the panel code results obtained by Yao et al. [43].

4.1.2.1. Tandem aerofoil configuration I

The wake pattern and the unsteady lift coefficient variation with time is obtained for the aerofoils at a 0.5c horizontal gap, 0.2c gap and 0 decalage with an angle of attack of 5 degrees and compared to the panel code results obtained by Yao et al. shown in the figure 21 [43]. The wake pattern obtained by the developed model is shown in the figure 22. An excellent qualitative agreement with the wake patterns is observed.
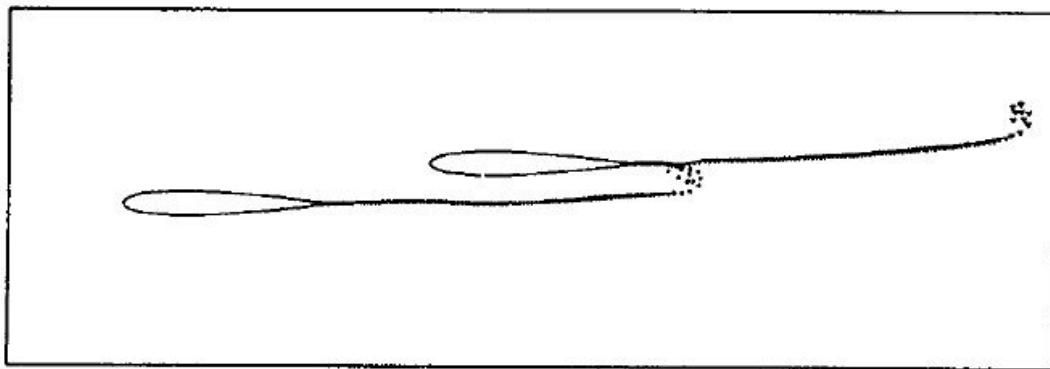
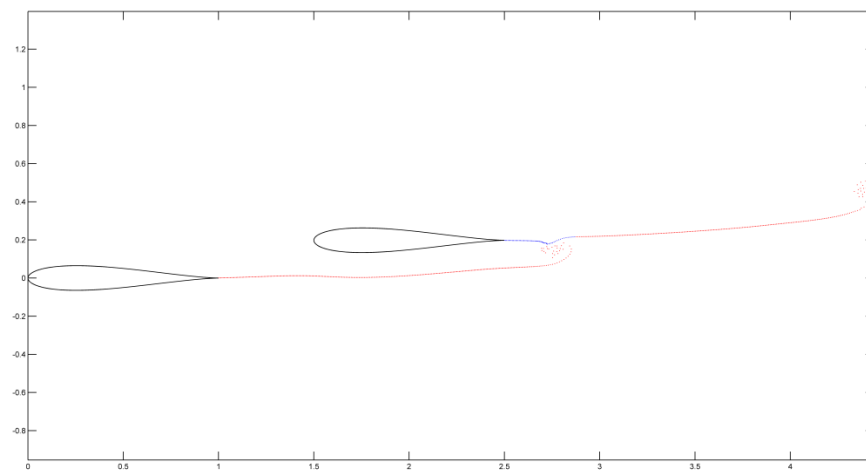*Figure 21:* wake pattern obtained by Yao et al. [24] for gap - 0.2c, horizontal gap - 0.5c

Figure 22: wake pattern for gap - 0.2c, horizontal gap - 0.5c, AOA - 5^0

The lift coefficients of the front and rear aerofoils are also obtained using the developed model and compared with the data obtained by Yao et al. [43]. The plots between unsteady lift coefficient and the non-dimensionalized time show a good qualitative and the quantitative agreement as shown in the figure 23.

Figure 23: comparison of the unsteady lift coefficient

4.1.2.2. **Tandem aerofoil configuration II**

The wake pattern and the unsteady lift coefficient variation with time is obtained for the aerofoils at a 0.5c horizontal gap, 0 gap and 0 decalage with an angle of attack of 5 degrees and compared to the panel code results obtained by Yao et al. [43] shown in

figure 24. The wake pattern obtained by the developed model is shown in the figure 25. An excellent qualitative agreement with the wake patterns is observed.

Figure 24: wake pattern obtained by Yao et al. [24] for gap **-** 0, horizontal gap **-** 0.5c

Figure 25: wake pattern for gap **-** 0, horizontal gap **-** 0.5c, AOA **-** 5^0

The lift coefficients of the front and rear aerofoils are also obtained using the developed model and compared with the data obtained by Yao et al. [43]. The plots between unsteady lift coefficients and the non-dimensionalized time show a good qualitative and the quantitative agreement as shown in the figure 26.
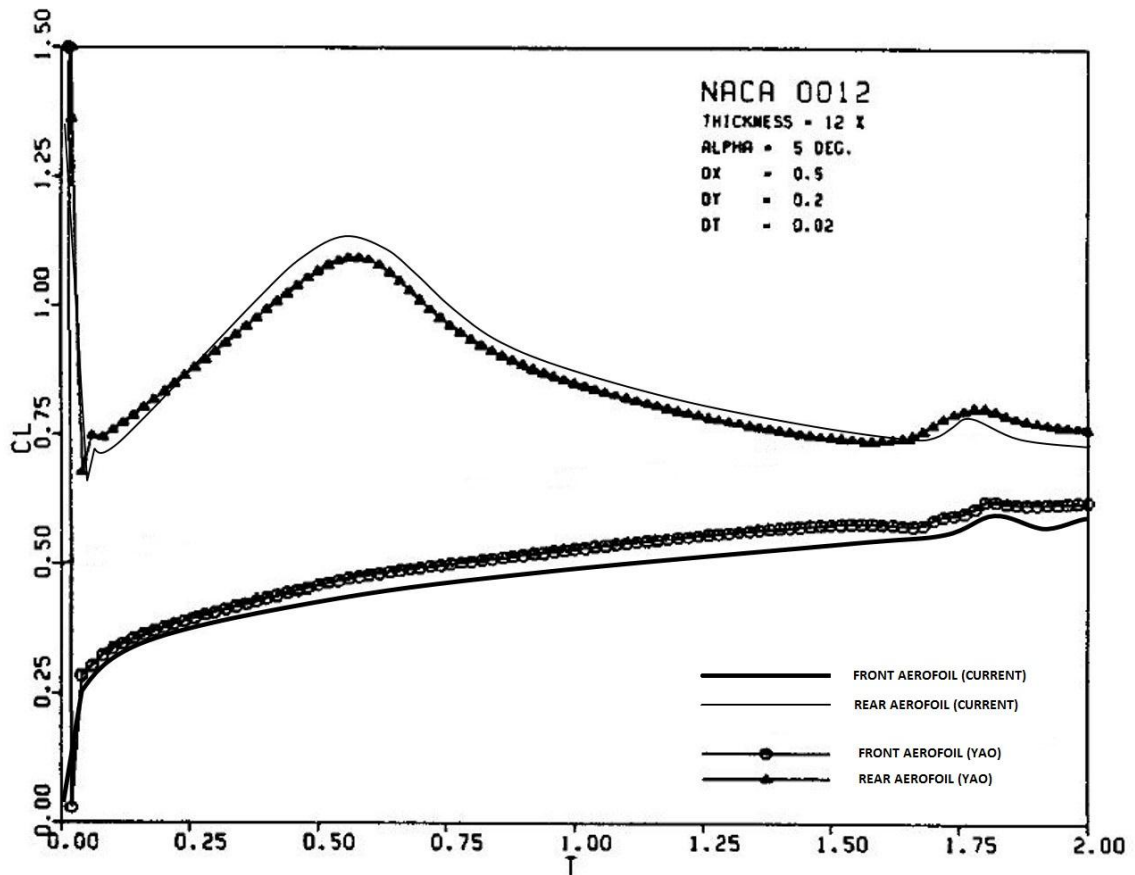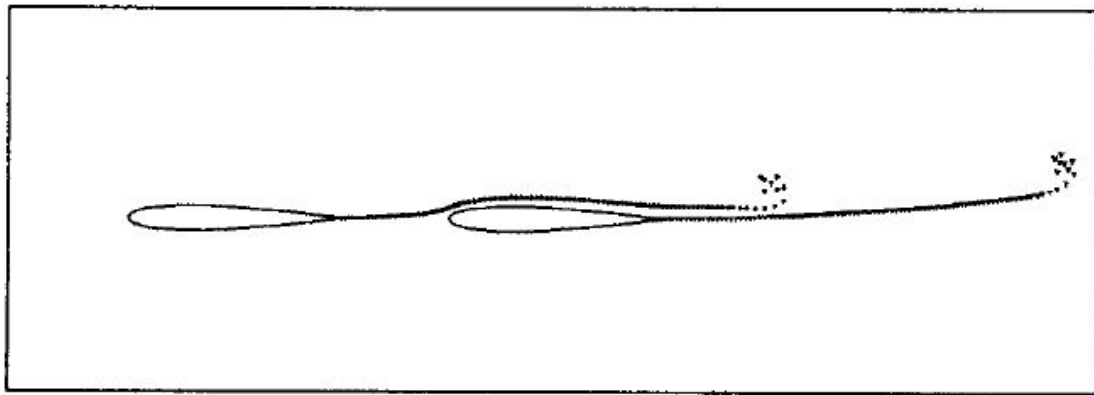

Figure 26: comparison of the unsteady lift coefficient

4.1.2.3. Tandem aerofoil configuration III

The wake pattern and the unsteady lift coefficient variation with time is obtained for the aerofoils at a 0.5c stagger, -0.2c gap and 0 decalage with an angle of attack of 5 degrees and compared to the panel code results obtained by Yao et al. shown in the figure 27

[43]. The wake pattern obtained by the developed model is shown in the figure 28. An excellent qualitative agreement with the wake patterns is observed.

Wake Pattern at
$\Delta x = 0.5c, \Delta y = -0.2c$
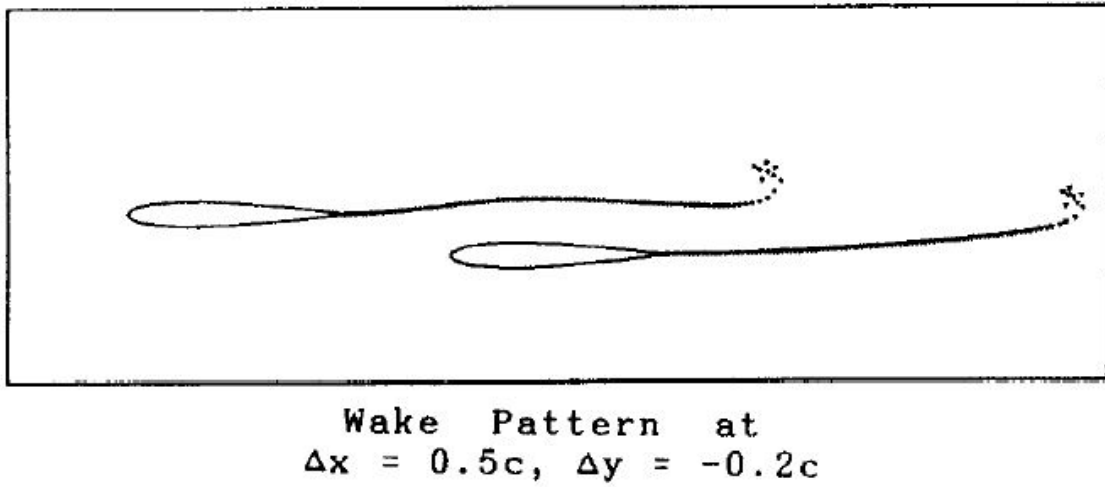
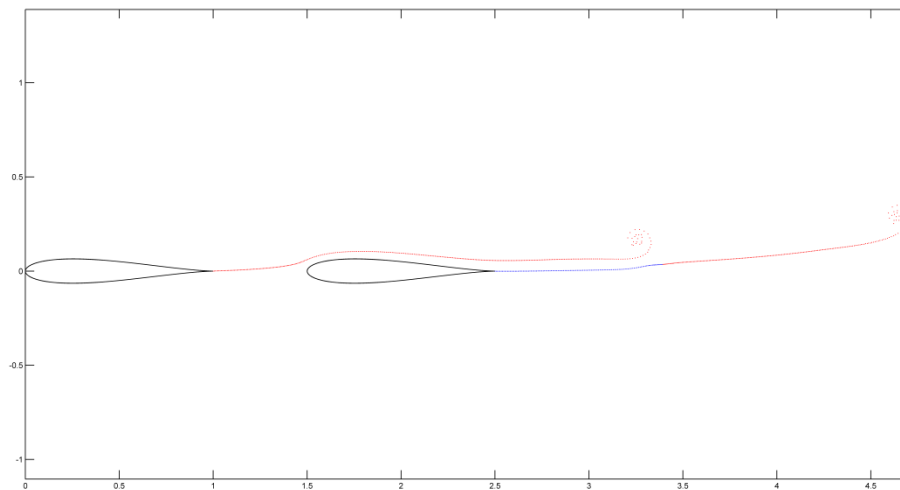*Figure 27:* wake pattern obtained by Yao et al. [24] for gap - -0.2c, stagger - 0.5c
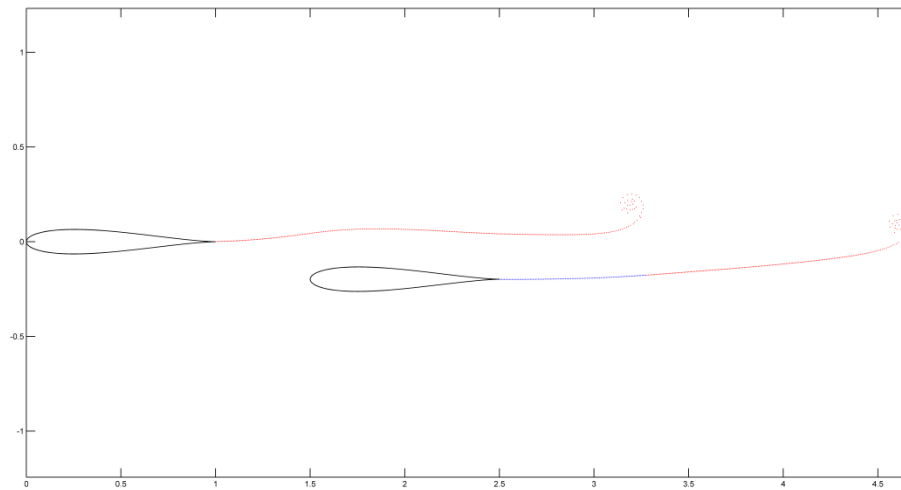
Figure 28: wake pattern for gap - -0.2c, horizontal gap - 0.5c, AOA - 5^0

The lift coefficients of the front and rear aerofoils are also obtained using the developed model and compared with the data obtained by Yao et al. [43]. The plots between unsteady lift coefficients and the non‑dimensionalized time show a good qualitative and the quantitative agreement as shown in the figure 29.
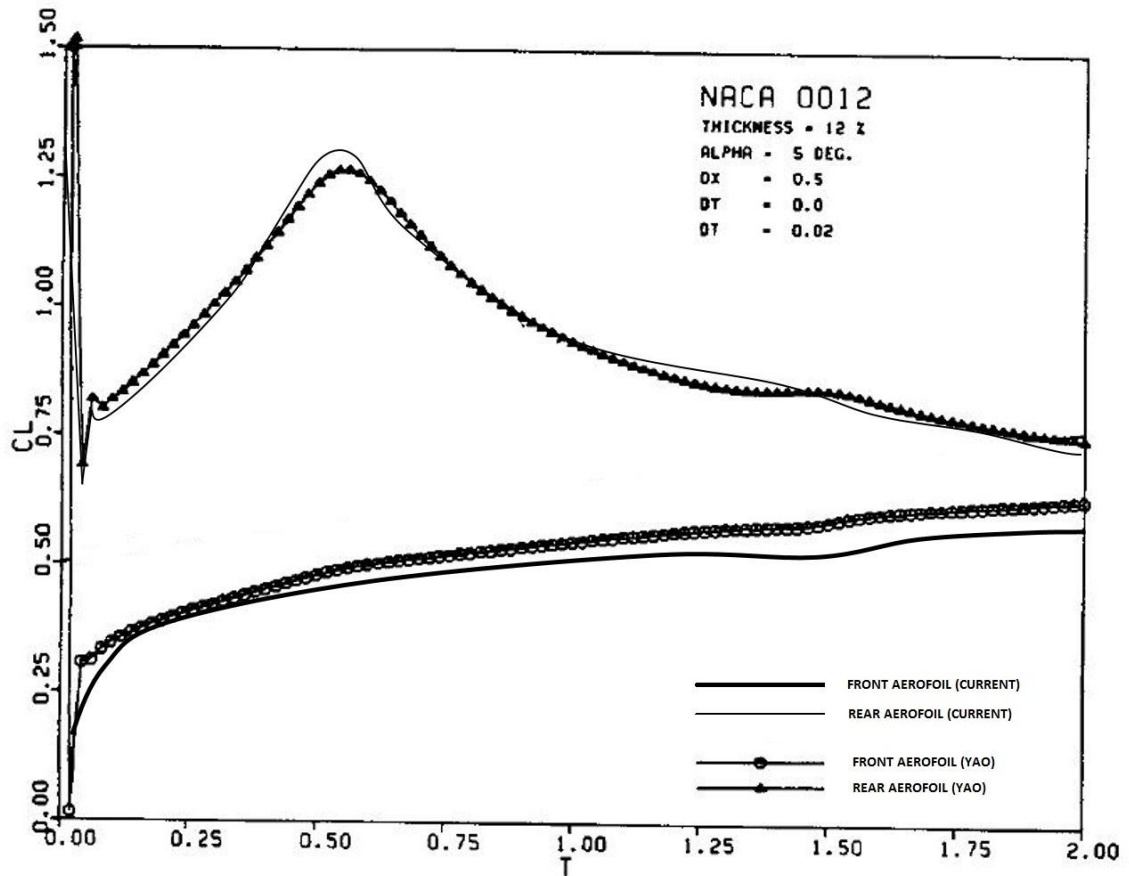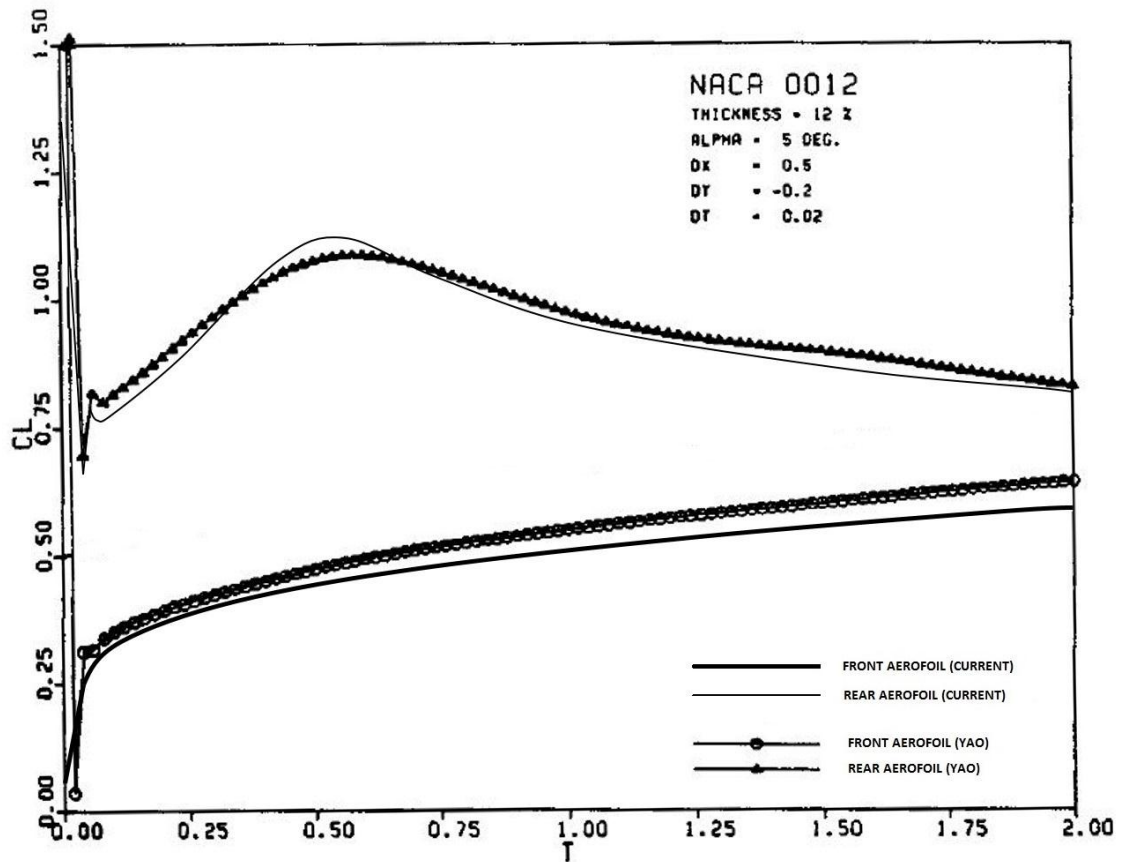

Figure 29: comparison of the unsteady lift coefficient

4.2. New results obtained by the developed model

4.2.1. Single stationary aerofoil

The flow filed of a single NACA 0012 aerofoil in a uniform stream is obtained as shown in the figure 30. To model the flow field of a stationary aerofoil in a uniform flow, the gap of the aerofoils in the doubly connected domain is taken to be 50 times the chord length. The magnitude of the gap prevents the influence of the bound vortex around one aerofoil on the other. This leads to a better prediction of the flow field around a single stationary aerofoil. The angle of attack is kept at 5 degrees and the variation of the ratio of the lift coefficient (C_l) to steady state lift coefficient (C_{ls}) is plotted with the non-dimensionalized time. The non-dimensionalized time step was taken to be 0.01.
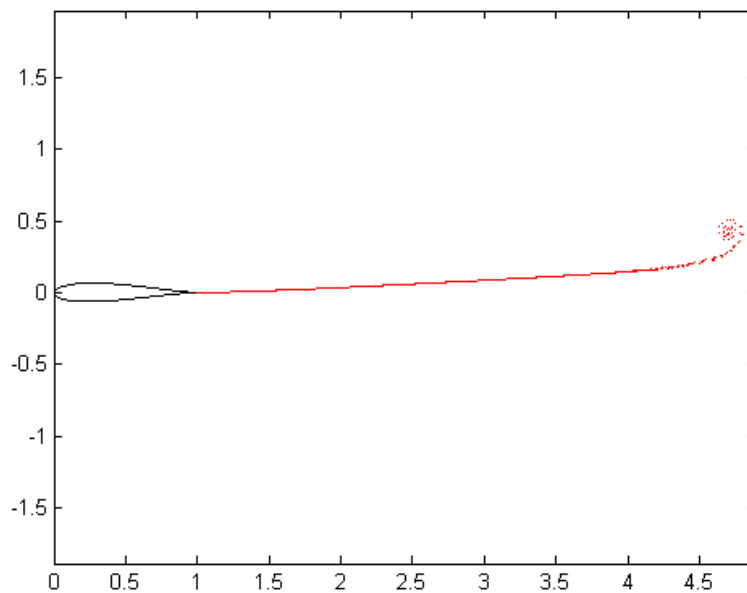
Figure 30: Single aerofoil in a uniform flow
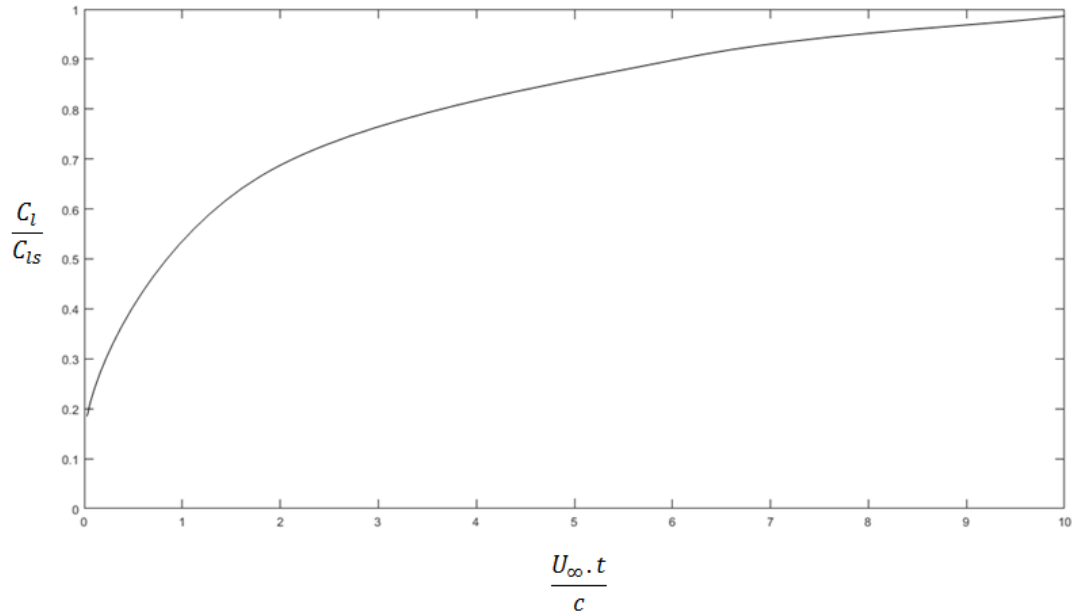
Figure 31: Plot of ratio of lift coefficient to steady state lift coefficient to non-dimensionalized time

4.2.2. <u>Single plunging aerofoil</u>

Variation of the lift coefficient with time is obtained for a single plunging aerofoil at different plunging amplitudes as shown in the figure 32. As in the case of single stationary aerofoil, the aerofoils are kept 50 times the chord length to avoid the influence of the bound vortices on one another since it leads to accurate predictions of the flow field for a single plunging aerofoil.

The plunging amplitudes and the reduced frequency are taken to be 0.025, 0.05, 0.075 and 4 respectively. The magnitudes of the plunging amplitudes are taken to be low values to avoid the leading edge vortex formation. The Kutta condition cannot be applied at the leading edge due to the absence of the sharp leading edge. Therefore a vortex shedding mechanism cannot be introduced at the leading edge. The limitation of no leading edge vortex formation is present in the current model.
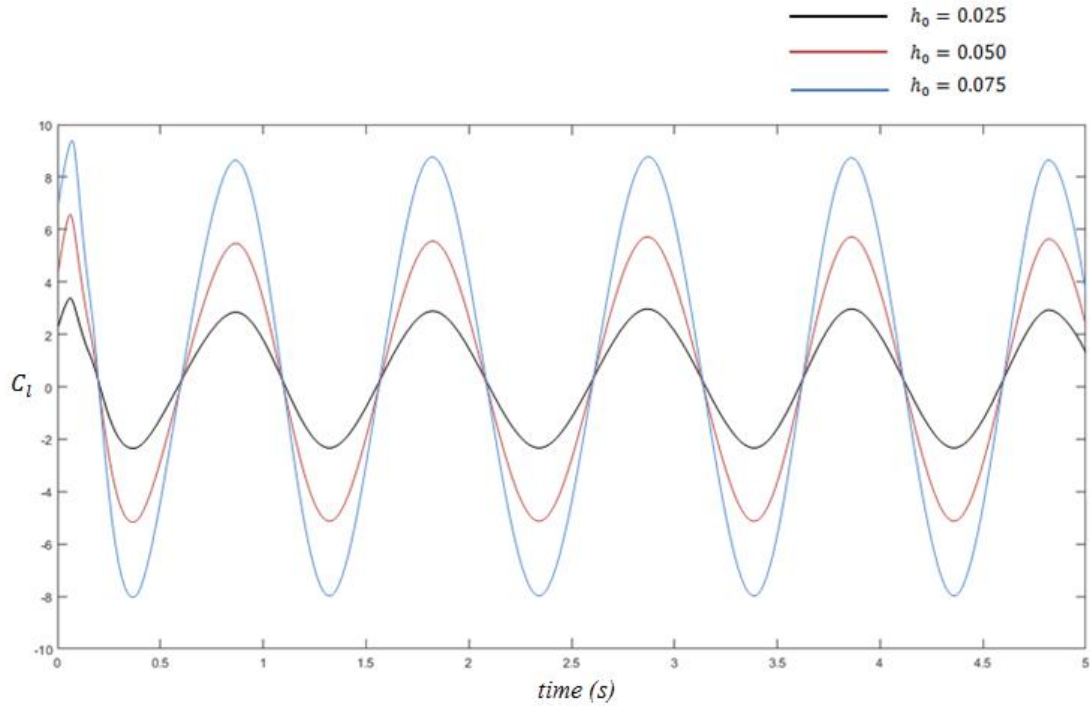
Figure 32: Variation of the lift coefficient with the time for different plunging
amplitudes, 0.025, 0.05 and 0.075

4.2.3. <u>Tandem aerofoils</u>

Using the developed model, the validated results for tandem aerofoils are extended for
different gaps. The variations of the lift coefficients and the non-dimensionalized time
for tandem aerofoils at different gaps are obtained as shown in figure 33, figure 34 and
figure 35. The angle of attack is taken to be 5 degrees for all the cases. The gaps are
taken to be 2, 3 and 4 times the chord length. The non-dimensionalized time step taken
to be 0.001 for a higher accuracy level. As opposed to the validation results for tandem
aerofoils, here the results are obtained for a longer non-dimensionalized time, from 0 to
10, for a better analysis.

Figure 33: Variation of the lift coefficient with non-dimensionalized time for tandem aerofoils at a 2c distance apart

Figure 34: Variation of the lift coefficient with non-dimensionalized time for tandem aerofoils at a 3c distance apart

Figure 35: Variation of the lift coefficient with non-dimensionalized time for tandem
aerofoils at a 4c distance apart

5. <u>CONCLUSION AND RECOMMENDATIONS</u>

5.1. <u>Conclusions</u>

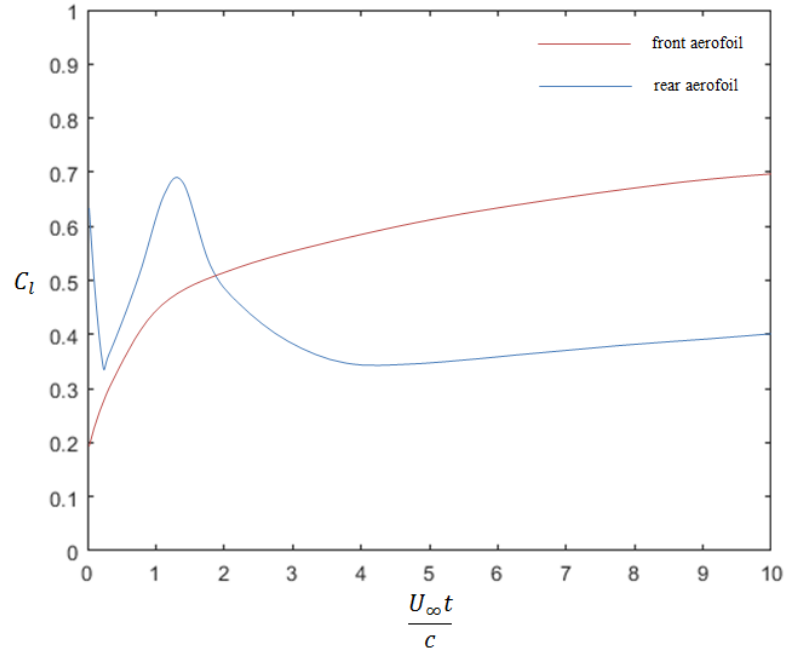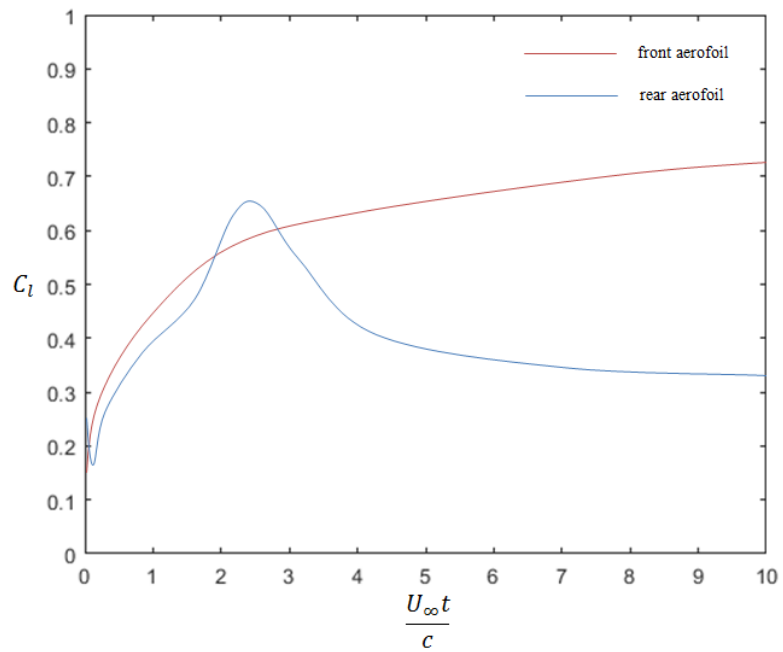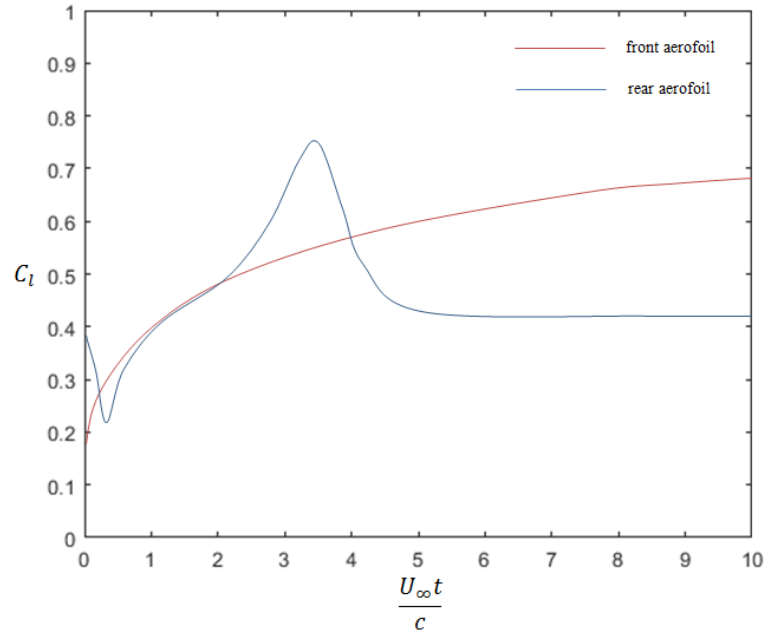An inviscid analytical-numerical model is developed for predicting unsteady forces in two aerofoil configurations. Using the developed model, aerofoils configurations in tandem and single stationary/ plunging aerofoil are analyzed. The qualitative agreement of the plunging aerofoil with the experimental and panel code data is excellent. It can be concluded that the wake pattern of a plunging aerofoil in a real fluid is mainly governed as an inviscid flow since the experimental data has an excellent qualitative agreement with the inviscid wake pattern. The obtained flow field for plunging aerofoil is a jet like, thrust producing flow field since the upper row of vortices have a counter clockwise rotation which indicates that the flow pattern is thrust producing. It is also observed that when the aerofoils are 50c distance apart from each other the influence of the vortices emitted by each aerofoil on the other aerofoil can be neglected.

An excellent agreement of the wake structure of the several tandem aerofoil configurations can be observed with the past literature. A good qualitative agreement can be observed when comparing unsteady forces in tandem aerofoil configurations. It is also observed that the different positions of the rear aerofoil in the tandem configuration do not affect the lift coefficient of the front aerofoil. However, the lift on the rear aerofoil varies with its relative position. Rear aerofoil gains its maximum lift when the starting vortex of the front aerofoil is in the vicinity of the leading edge of the rear aerofoil. It can be seen that the lift of the rear aerofoil is increased by placing it in a proper position as shown in the figure 26. The interaction of the starting vortex of the front aerofoil and the starting vortex of the rear aerofoil seems to reduce the lift of the rear aerofoil while approximately not changing the lift of the front aerofoil.

The results obtained for a single aerofoil in a uniform flow shows that the as the initial vortex moves away from the aerofoil, the lift force enhances and the plot in figure 31

shows that the ration of the lift coefficient and the steady state lift coefficient tends to 1 as expected which is the steady state of the flow field.

In the case of single plunging aerofoil, the magnitudes of the plunging amplitudes are carefully selected to avoid leading edge vortex formation. The developed model is not valid for the cases when the leading edge vortices are present in the flow field. This is due to the inability to model the leading edge vortex in the developed model. The values of the lift coefficients are periodic with the same period for the three cases since the reduced frequency is the same for all the amplitudes. The variation of the lift coefficient increases as the plunging amplitude increases. Negative and positive lift coefficients can be observed for the upward and the downward stokes respectively.

It can be observed that the results obtained for tandem aerofoils at different gaps have many things in common. There is a peak in lift coefficient in the rear aerofoil in all configurations. When the starting vortex emitted by the front aerofoil moves above the rear aerofoil a low pressure region is created in that region. This causes the lift on the rear aerofoil to spike up. As the vortex moves with the flow passing the rear aerofoil, the lift decreases since the pressure increases above the rear aerofoil. As opposed to the case of 0.5c gap the lift coefficient of the front aerofoil is greater than that of the rear aerofoil when the non-dimensionalized time increases. As shown in figure 33, figure 34 and figure 35 when the non-dimensionalized times are approximately greater than 2, 3 and 4 the lift coefficients of the front aerofoil becomes greater than that of rear aerofoil for the gaps 2c, 3c and 4c respectively. The peaks of the lift coefficient of the rear aerofoil occur when the non-dimensionalized times 1.5, 2.5, 3.5 for gaps are 2c, 3c and 4c respectively. This is due to the fact that as the gap between aerofoils increases the time required for the starting vortex, generated by front aerofoil, to travel above the rear aerofoil increases. Also the results show that the lift coefficients converge as the time increases (systems achieve steady state).

5.2. <u>Recommendations for Future work</u>

Since the leading edge of the aerofoils do not have any sharp edges, the analytical-Numerical approach does not include the generation of the leading edge vortex which is very important analyzing flapping motions of aerofoil configurations. A leading edge vortex can be introduced to the flow field if there's a sharp edge at the leading edge of the aerofoil. Therefore modeling the flow field for two flat plates is recommended as a future work.

In the study, only synchronized plunging motion is considered when predicting unsteady forces. The study can be extended to asynchronized plunging motion, pitching motion in the same phase and counter phase, and combined pitch and plunge motion in counter phase. Then the complex potential associated with the moving bodies can be evaluated using a suitable Laurent series expansion.

Finally the developed model capable of determining unsteady forces can be used to optimize flapping wing parameters in a biplane configuration.

REFERENCES

[1] L. Prandtl, "Induced Drag of Multiplanes," *NACA TN*, vol. 182, Mar. 1924.

[2] J.M. Moschetta and C. Thipyopas, "Aerodynamic Performance of a Biplane Micro Air Vehicle," *J. Aircr.*, vol. 44, no. 1, pp. 291–299, 2007.

[3] J. Wolkovitch, "Subsonic VSTOL Aircraft Configurations with Tandem Wings," *J. Aircr.*, vol. 16, no. 9, pp. 605–611, 1979.

[4] M. D. Rhodes and B. P. Selberg, "Benefits of dual wings over single wings for high-performance business airplanes," *J. Aircr.*, vol. 21, no. 2, pp. 116–127, 1984.

[5] M. Kaya, I. H. Tuncer, K. D. Jones, and M. F. Platzer, "Optimization of Flapping Motion Parameters for Two Airfoils in a Biplane Configuration," *J. Aircr.*, vol. 46, no. 2, pp. 583–592, 2009.

[6] P. G. Ifju, D. A. Jenkins, S. Ettinger, Y. Lian, W. Shyy, and M. R. Waszak, "Flexible-Wing-Based Micro Air Vehicles," *Am. Inst. Aeronaut. Astronaut.*, vol. 705, pp. 1–11, 2002.

[7] W. Shyy, Y. Lian, J. Tang, D. Viieru, and H. Liu, *Aerodynamics of Low Reynolds Number Flyers*. Cambridge University Press, 2007.

[8] G. K. Taylor, R. L. Nudds, and A. L. R. Thomas, "Flying and swimming animals cruise at a Strouhal number tuned for high power efficiency," *Nature*, vol. 425, no. 6959, pp. 707–711, Oct. 2003.

[9] A. A. Tchieu, D. Crowdy, and A. Leonard, "Fluid-structure interaction of two bodies in an inviscid fluid," *Phys. Fluids 1994-Present*, vol. 22, no. 10, p. 107101, Oct. 2010.

[10] R. I. Lewis, *Vortex Element Methods for Fluid Dynamic Analysis of Engineering Systems*. Cambridge University Press, 2005.

[11] P. Ramachandran, M. Ramakrishna, and S. C. Rajan, "Efficient random walks in the presence of complex two-dimensional geometries," *Comput. Math. Appl.*, vol. 53, no. 2, pp. 329–344, Jan. 2007.

[12] M. E. Klonowska and W. J. Prosnak, "On an effective method for conformal mapping of multiply connected domains," *Acta Mech.*, vol. 119, no. 1–4, pp. 35–52, Mar. 1996.

[13] D. Crowdy, "A new calculus for two-dimensional vortex dynamics," *Theor. Comput. Fluid Dyn.*, vol. 24, no. 1–4, pp. 9–24, Apr. 2009.

[14] L. M. Milne-Thomson, *Theoretical Hydrodynamics*. Courier Corporation, 1968.

[15] D. J. Acheson, *Elementary Fluid Dynamics*. Clarendon Press, 1990.

[16] K. K. M. N. P. Samaraweera, M. A. C. K. Gunarathna, and K. A. L. Kollure, "An inviscid model for unsteady flow in multiply connected domains," *Eur. J. Mech. - BFluids*, vol. 41, pp. 123–132, Sep. 2013.

[17] D. F. Scharpf and T. J. Mueller, "Experimental study of a low Reynolds number tandem airfoil configuration," *J. Aircr.*, vol. 29, no. 2, pp. 231–236, 1992.

[18] R. Knoller, "Die Gesetze des Luftwiderstandes," *Flug- Mot. Wein*, vol. 03, no. 21, pp. 1–7.

[19] A. Betz, "Ein Beitrag zur Erklarung des Segeluges," *Z. Flugtech. Mot.*, pp. 269–272, Jan. 1912.

[20] R. Katzmayr, "Effect of periodic changes of angle of attack on behavior of airfoils," Oct. 1922.

[21] K. D. Jones, C. M. Dohring, and M. F. Platzer, "Experimental and Computational Investigation of the Knoller-Betz Effect," *AIAA J.*, vol. 36, no. 7, pp. 1240–1246, 1998.

[22] *Aerodynamic Theory: General aerodynamic theory : Perfect fluids / [By] Th. von Kármán ; J. M. Burgers*. J. Springer, 1935.

[23] I. E. Garrick, "Propulsion of a flapping and oscillating airfoil," Jan. 1937.

[24] Z. YAO, P. GARCIA-FOGEDA, D. LIU, and G. SHEN, "Vortex/wake flow studies for airfoils in unsteady motions," in *7th Applied Aerodynamics Conference*, American Institute of Aeronautics and Astronautics.

[25] H. Aziz and R. Mukherjee, "Unsteady Aerodynamics of Multiple Airfoils in Configuration," *Am. Inst. Aeronaut. Astronaut.*

[26]   W. Hicks, "On the motion of two cylinders in a fluid," *Q. J. Pure Appl. Math.*, vol. 16, pp. 113–140, 193–219, 1879.

[27]   A. Greenhill, "Functional images in Cartesians," *Q. J. Pure Appl. Math.*, vol. 18, pp. 356–362, 1882.

[28]   L. H. Carpenter, "On the Motion of Two Cylinders in an Ideal Fluid around Two Moving Bodies," *J. Res. Natl. Bur. Stand.*, vol. 61, pp. 83–87, 1958.

[29]   M. Kawaguti, "The Flow of a Perfect Fluid around Two Moving Bodies," *J. Phys. Soc. Jpn.*, vol. 19, no. 8, pp. 1409–1415, Aug. 1964.

[30]   M. Lagally, "Die reibungslose Strömung im Außengebiet zweier Kreise .," *ZAMM - J. Appl. Math. Mech. Z. Für Angew. Math. Mech.*, vol. 9, no. 4, pp. 299–305, Jan. 1929.

[31]   C. Ferrari, "Sulla trasformazione conforme di due cerchi in due profili alari," *Memoire Della R. Accad Della Sci. Torino*, 1930.

[32]   E. T. Whittaker and G. N. Watson, *A Course of Modern Analysis*, 4 edition. Cambridge University Press, 1927.

[33]   I. E. Garrick, "Potential flow about arbitrary biplane wing sections," Jan. 1937.

[34]   Q. X. Wang, "Interaction of two circular cylinders in inviscid fluid," *Phys. Fluids 1994-Present*, vol. 16, no. 12, pp. 4412–4425, Dec. 2004.

[35]   D. G. Crowdy, "Analytical solutions for uniform potential flow past multiple cylinders," *Eur. J. Mech. - BFluids*, vol. 25, no. 4, pp. 459–470, Jul. 2006.

[36]   H. F. Baker and I. Krichever, *Abelian Functions: Abel's Theorem and the Allied Theory of Theta Functions*. Cambridge, Eng. ; New York: Cambridge University Press, 1996.

[37]   D. A. Hejhal, *Theta functions, kernel functions, and Abelian integrals*. American Mathematical Society, 1972.

[38]   E. J. Routh, "Some applications of conjugate functions," *Proc. Lond. Math. Soc.*, vol. 12, pp. 73–89, 1881.

[39]   C. C. Lin, "On the Motion of Vortices in Two Dimensions: I. Existence of the Kirchhoff-Routh Function," *Proc. Natl. Acad. Sci. U. S. A.*, vol. 27, no. 12, pp. 570–575, Dec. 1941.

[40]   C. C. Lin, "On the Motion of Vortices in Two Dimensions: II. Some Further Investigations on the Kirchhoff-Routh Function," *Proc. Natl. Acad. Sci. U. S. A.*, vol. 27, no. 12, pp. 575–577, Dec. 1941.

[41]   E. R. Johnson and N. R. McDonald, "The motion of a vortex near two circular cylinders," *Proc. R. Soc. Lond. Math. Phys. Eng. Sci.*, vol. 460, no. 2044, pp. 939–954, Apr. 2004.

[42]   L. Zannetti, F. Gallizio, and G. M. Ottino, "Vortex motion in doubly connected domains," *J. Fluid Mech.*, vol. 612, pp. 143–152, Oct. 2008.

[43]   D. G. Crowdy and J. S. Marshall, "The motion of a point vortex around multiple circular islands," *Phys. Fluids 1994-Present*, vol. 17, no. 5, p. 056602, May 2005.

[44]   D. G. Crowdy and J. S. Marshall, "Analytical formulae for the Kirchhoff–Routh path function in multiply connected domains," *Proc. R. Soc. Lond. Math. Phys. Eng. Sci.*, vol. 461, pp. 2477–2501, 2005.

[45]   D. Gaier, *Konstruktive Methoden der konformen Abbildung*. Springer-Verlag, 2013.

[46]   D. Crowdy, "Calculating the lift on a finite stack of cylindrical aerofoils," *Proc. R. Soc. Lond. Math. Phys. Eng. Sci.*, vol. 462, no. 2069, pp. 1387–1407, May 2006.

[47]   R. R. Clements, "An inviscid model of two-dimensional vortex shedding," *J. Fluid Mech.*, vol. 57, no. 02, pp. 321–336, Feb. 1973.